

# Modeling the Heterogeneity in COVID-19's Reproductive Number and Its Impact on Predictive Scenarios

Claire Donnat

Susan Holmes

cdonnat@stanford.edu

susan@stat.stanford.edu

Department of Statistics, Stanford University  
390 Jane Stanford Way, Stanford CA 94305, USA

## Abstract

The correct evaluation of the reproductive number  $R$  for COVID-19 —which characterizes the average number of secondary cases generated by each typical primary case— is central in the quantification of the potential scope of the pandemic and the selection of an appropriate course of action. In most models,  $R$  is modeled as a “universal” constant for the virus across outbreak clusters and individuals — effectively averaging the effect of the inherent variability of the transmission process due to varying population densities, demographics, temporal factors, etc. Yet, due to the exponential nature of epidemics growth, this simplification can lead to inaccurate predictions and/or risk evaluation, thus begging the question: how large is the impact of this simplification on predictions and risk estimates? How can this variability be percolated in the projections for the pandemics so as to provide a more accurate uncertainty quantification? In this perspective, instead of considering a single, fixed  $R$ , we model the reproductive number as a distribution sampled from a simple Bayesian hierarchical model. Using our fitted model, we then simulate the spread of the epidemic as well as the impact of different social distancing strategies, and highlight the strong impact of this added variability on the reported results. We emphasize that our goal is not to replace benchmark methods for estimating the reproductive numbers, nor to pretend to more accurate predictive scenarios. Rather, we focus solely on discussing the importance of the impact of  $R$ 's heterogeneity on uncertainty quantification for the current

COVID-19 pandemic.

Bayesian Statistics | Epidemiology | Contagion Models | COVID-19

## 1 Introduction

First detected in Wuhan (Hubei Province, China) in December 2019, the current COVID-19 pandemic has thrown the entire world in a state of turmoil, as governments closely monitor the spread of the virus and have taken unprecedented measures to contain local contagion outbreaks. In order to adequately inform public policy makers, experts in epidemiology are currently trying to assess the potential scope of this global pandemic and to draw predictive scenarios. In this context, much attention has especially been drawn to the monitoring of one quantity: the pandemic’s reproductive number  $R$ , which appears as a key parameter in almost all contagion models — whether these scenarios are drawn using variants of the Susceptible-Exposed-Infected-Removed (SEIR) deterministic equations [7, 8, 12, 10] or of exponential growth models [13].

By definition, the reproductive number  $R$  characterizes the expected number of secondary cases produced by one single typical infectious case. This quantity can be further broken down into different categories. Experts typically distinguish the  $R_0$  (basic reproductive number) — which assumes that the population is completely susceptible and is well adapted to the modeling of a completely novel virus — and a broader “effective”  $R$ , which assumes a mixed population of susceptible and immune hosts. For the sake of clarity, this paper will focus on discussing the latter, but our discussion is also applicable to the  $R_0$ . To give more intuition on the underlying transmission mechanisms that it captures, the reproductive number  $R$  can be decomposed as the product of three terms [3]:

$$R = \tau \bar{c} D_I \tag{1}$$

where  $\tau$  is the transmissibility (i.e., probability of infection given contact between a susceptible and infected individual),  $\bar{c}$  is the average number of contact per day between susceptible and infected individuals, and  $D_I$  is the duration of infectiousness — that is, the number of days during which

an infected patient can be expected to contaminate others.  $R$  thus serves as an epidemiological metric to describe the contagiousness or transmissibility of infectious agents: the outbreak is expected to continue if  $R$  is greater than 1, or to naturally subside if  $R$  is strictly less than 1. As recently highlighted by Delameter et al. [4], this coefficient inherently depends on some local characteristics of the population. In particular, going back to the decomposition provided in Eq. 1,  $R$  is intrinsically tied to temporal and spatial-varying factors, such as population age demographics, political or environmental variables, cultural or social dynamics, or the density of the population — all favoring or diminishing the rate of contacts  $\bar{c}$  between individuals.  $R$  can thus be naturally modeled using a hierarchical framework, which accounts for the reproductive number's heterogeneity by decomposing it according to different strata. For instance, the reproductive number  $R$  could be hierarchically broken down according to countries (or regions), age groups, and, at the most granular level, across subjects. The expected number of secondary cases is indeed contingent on each primary cases' socio-economic status, age, etc., and perhaps even time — as one could imagine the contact rates varying between weekends and weekdays. A very fine-grain analysis of the  $R$ 's heterogeneity would thus model  $R$  as a distribution over cases and time in a given population. Figure 1 shows one such potential hierarchical stratification.

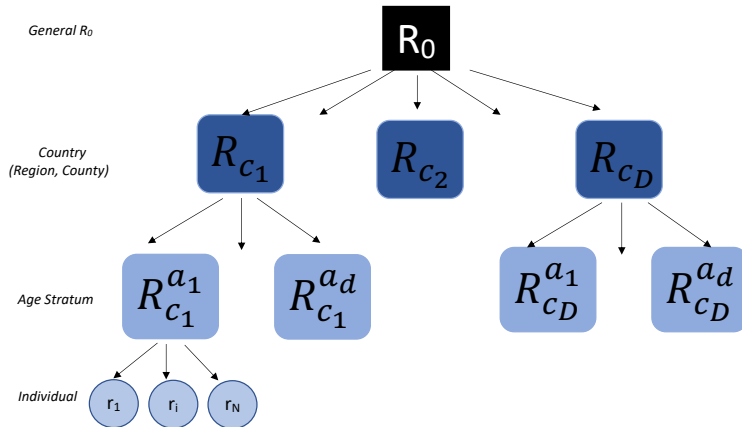


Figure 1: Hierarchical model for the reproductive number  $R$

The “universal”  $R$  used in epidemiological models to characterize the disease might thus be thought of as a general summary statistic, averaged over individuals and populations — thus discarding any

form of local variability or hierarchical organization. In the standard framework, the heterogeneity of  $R$  is partially accounted for by fitting the model to local data (typically at the country or county level), but thus effectively (a) discarding information that could be shared across groups by fitting each local model independently and (b) neglecting the inherent variability in this coefficient at the individual level. The latter can in particular become problematic, due to the exponential nature of the epidemics growth — a phenomenon that we propose to investigate here.

The underlying motivation behind the simplification of the random  $R$  to a constant value lies in the assumption that the dynamics of the pandemic are similarly described by the trajectory estimated using the average  $R$ , or the average of the epidemic’s trajectories with varying  $R$ . Yet, because the number of new incident cases each day depends exponentially on the history of the trajectory, this averaging approximation might come at a huge accuracy cost in prediction models. To give a clearer picture of the potential effects of this additional randomness on the model, let us consider two naive experiments.

**First Experiment: Inherent effect of the randomness on the model.** In the first experiment, we consider a simplification of the exponential growth model for an epidemic. In this model, for a given reproductive number  $R$ , each new infectious case generates a  $\text{Poisson}(R)$  number of new cases the following day. This amounts to considering an instantaneous incubation period and that each primary case is only contagious for day. At each time  $t$ , the number of new cases is thus generated as:

$$X_{t+1} = \text{Poisson}(RX_t)$$

We assume that exactly 1% of these incident cases will not recover from the disease, so that the cumulative number of deaths at time  $t$  can be written as  $D_t = 0.01 \sum_{s=1}^t X_s$ .

Let us now investigate how the error induced by considering a fixed  $R$  instead of a random one is exponentially propagated throughout the projected trajectory for the epidemic. In particular, we show that this approximation can potentially lead to (a) an increased variability of the number of deaths  $D_t = 0.01 \sum_{s=1}^t X_s$  and (b) the introduction of new “worst cases scenarios”. Consider for instance the stopping time corresponding to the total number of deaths reaching 5,000:

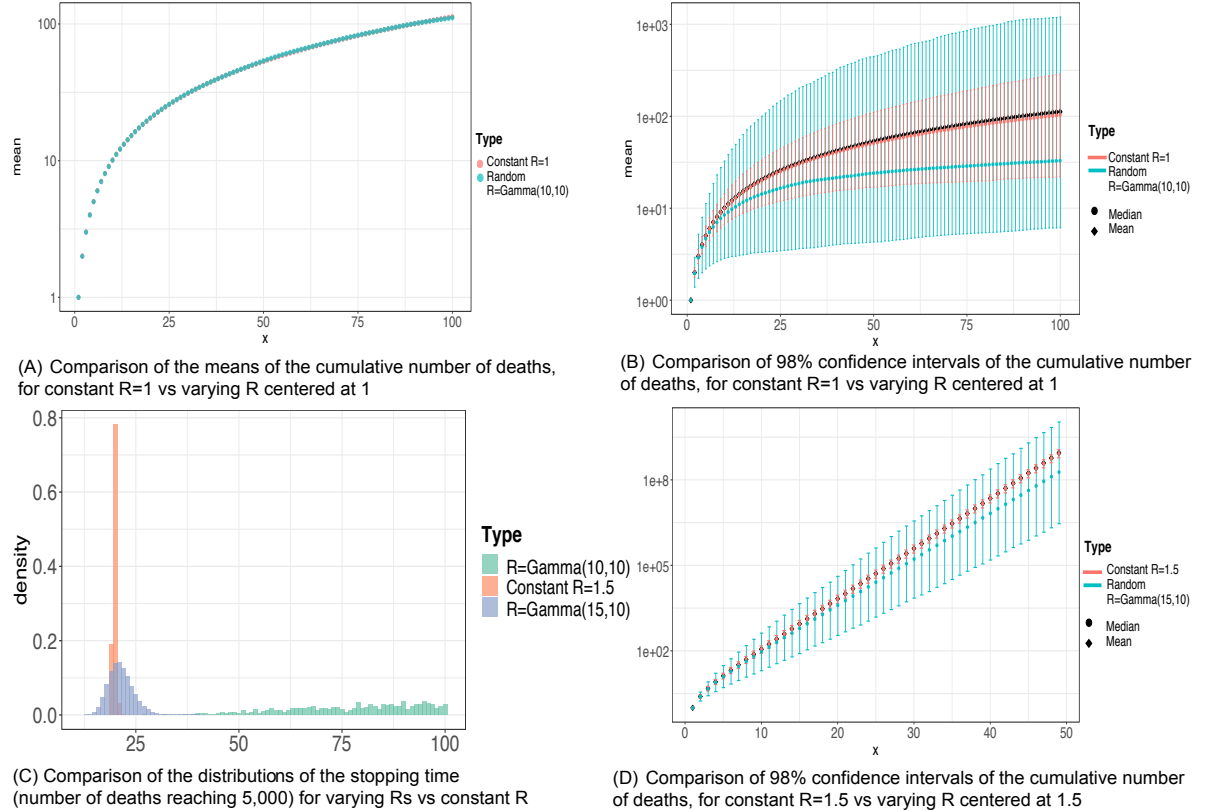


Figure 2: Output of simulations showing comparisons of the possible trajectories for contagion models using fixed  $R_0$  vs variable  $R$ . Dots indicate the average predicted values, whereas the error bars represent the 98%-confidence interval.

$\tau = \min\{t \in \mathbb{N} : D_t \geq 5,000\}$ . Since the model is build sequentially, it is difficult to get close form formulas and exact probabilistic results. We thus resort to simulating 40,000 contagion events over 100 days to quantify the impact of this added variability. In one case, we simulate the propagation of the epidemic using a fixed, constant  $R_0$ . In the other, we simulate the propagation assuming that at each time step,  $R$  is sampled from a gamma distribution centered around  $R_0$ . We compare the effect of the two models on the evolution of the number of deaths and the stopping time  $\tau$ . The results are reported in Figure 2.

Based on those simulations, we make two observations: (a) while the mean number of deaths

is roughly the same for both scenarios (Fig 2A), the distributions are substantially different (Fig 2B,D). In particular, the worse-case scenario (99th quantile) is bigger by orders of magnitude when considering a variable  $R$ , with respect to its constant counterpart. This is an important observation: average predictions for the fixed and variable  $R$  models are seemingly the same, yet their associated uncertainty estimates and catastrophic scenarios are radically different. Moreover, for constant  $R_0 = 1$ , the stopping time  $\tau = \min\{t \in \mathbb{N} : D_t \geq 5,000\}$  is never reached. It is nonetheless reached in 0.19% of cases using a varying  $R$  (Fig 2C), thus making it a non-zero probability event and enlarging the space of possible events. The variable- $R$  model thus presents a wider scope of worst-case scenarios than the ones predicted using a constant, average  $R_0$  — a fact that is potentially crucial for policy makers to make informed decisions.

**Second Experiment: effect of the randomness on the estimation procedure.** We have shown that a constant  $R_0$  might not be satisfactory from the model’s perspective — we now also assess how the error induced by the averaging is also reverberated in the estimation procedure. In this second experiment, we simulate an exponential growth of the number of incident cases over the course of 20 days using a Gamma distributed  $R$  with shape 1.2 and scale 1. This is in fact mimicking a scenario under which  $R$  varies every day, thus accounting for some temporal effects (weekend vs week days), subject-effects across newly infected cases, etc. Let us now try to recover the  $R_0$  using the Exponential Growth model in the R0 R-package. The average difference between the recovered and true mean  $R_0$  over 1,000 simulations is 2.94 (with only 8.5 % coverage by the recovered confidence intervals)— that is, more than twice the 1.35 mean error that we obtain by simulating data under the same setting using a constant  $R_0 = 1.2$ . This brings to light two new observations: (a) standard  $R$  estimation procedures seem to perform even less well with variable  $R_0$ , and (b) the confidence intervals usually provided are too narrow, and do not correctly emphasize the high uncertainty of the predicted  $R$  value.

In light of these synthetic experiments, assuming the reproductive number  $R$  to be constant thus comes at a huge cost in terms of accuracy of the reported predictive scenarios. In particular, the worst-case scenarios associated to these predictions could be either (i) too optimistic without appropriately characterizing their uncertainty, (ii) unable to account for the existence of “super-spreaders” in the

general population, and (iii) fail to allow certain rare events leading to the formation of outbreaks — thus potentially misleading policy makers and begging the question: for the analysis of our real data, how much variability do we need to account for in the modeling of  $R$ ? Is the aggregated version sufficient to provide informative scenarios, or is a hierarchical model preferable?

From a statistical viewpoint, the issue of accounting for the  $R$ ’s variability can be tackled from two perspectives: (a) a “spatial random-effects” approach, splitting the data into groups in a hierarchical fashion and assuming the  $R_0$  to be constant within groups — the underlying assumption being that the within-group variance is significantly smaller than the global variance, and that this stratification thus reduces the error in the estimation of the uncertainty — or (b) a “full random-effects” model, incorporating both spatial and temporal variability. The latter builds upon the spatial random effects model, but adds a further layer of variability by assuming a random daily effect. In other words, whereas in the “spatial random-effects” approach, the  $R$  is assumed to vary across groups but is held constant throughout the trajectory, in the “full random-effects” model,  $R$  varies at each time step. This assumes that the inherent daily variations of the reproductive number  $R$ s are too substantial to be neglected. In both cases, a more granular estimation of the  $R$  using geographical, weekday, weather, and other sources of information could make day-to-day variations in the  $R$  provide more realistic epidemiological predictions of the outbreak propagation speed, as well as the expected times before hospitals reach capacity — both crucial quantities for informing policy makers as they arbitrate between different courses of action, especially as drastic public health measures typically come at significant social and economical costs. We emphasize that our goal here is not to come up with a new model or definition for the  $R$ , nor to pretend to a better predictive model than experts in epidemiology. Rather, our focus is simply to assess — as statisticians — the effect of this added variability in predictive scenarios, in order to grasp a little better how this variability is propagated in downstream analyses. One of the hypotheses that we would thus like to test is if the heterogeneity of the  $R$  coefficient can severely impact predictive scenarios for the outbreaks: how certain are we about the predictions that we are making? In light of the observed heterogeneity of the  $R$ ’s, how confident are we of the transferability of a given policy in one country to another?

In this paper, we deal with stochasticity and limited/missing data using a Bayesian perspective. We begin by describing the Bayesian hierarchical model that we use to estimate the varying reproductive

number  $R$ . This approach provides a more natural framework for uncertainty quantification through the provision of credible intervals. We show the impact of this variability on the predictive scenarios and the effect of public policy measures (e.g. social distancing or alternating lockdown days) that can be drawn using these models. All of our experiments here are deployed on the current COVID-19 pandemic. The code and data used for this analysis are openly available on the authors' Github<sup>1</sup>.

## 2 Model and Theory

Our evaluation of the effect of heterogeneity in predictive scenarios comprises of two steps, whose details are provided separately in the two following sections. The first consists in estimating the number of new cases (or incidence cases) per day, using a model for the heterogeneity of the reproductive number  $R$ . The second step models the hospital and ICU occupancy as a consequence of the surge in incident cases, which we detail in section 3. We propose to account for the heterogeneity of the reproductive number by dividing the data into geographical groups (Level 1 of the hierarchical framework presented in Figure 1), and compare the results for the spatial random-effects model with the ones obtained for the full random-effects model.

**Modeling an heterogeneous incidence proportion.** We base the first step of our analysis on a simple Bayesian hierarchical extension to models currently deployed throughout the literature to compute the  $R_0$ . The Bayesian formalism is indeed particularly amenable to uncertainty quantification and modeling with limited information (as we track the epidemic at various stages of progression across locations) through the use of priors and posterior credible intervals.

Throughout the remainder of this analysis, let us adopt the following formalism. Let  $G$  be the number of groups that we want to analyze (these could either be localized virus outbreak clusters, regions or countries). Let  $N_g$  denote the population of each of these groups, initially assumed to be completely susceptible. For the sake of simplicity, we neglect the number of births, natural deaths, and incoming/outgoing flux between groups.

---

<sup>1</sup>Code and data at: [https://github.com/donnate/heterogeneity\\_RO](https://github.com/donnate/heterogeneity_RO)

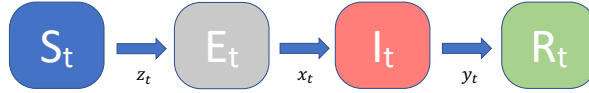


Figure 3: Compartmental SEIR model

*Literature Review.* The classical model for predicting the spread of an epidemic within each group is the Susceptible-Exposed-Infected-Removed (SEIR) compartmental model, which was used to estimate COVID19’s  $R_0$  in its early days [12]. In this setting, each group of size  $N_g$  is split in one of four different compartments (see Figure 3): people are either susceptible, exposed, infected (which we understand as exhibiting symptoms) or removed (including recoveries and deaths). The SEIR is thus a deterministic model, in which the evolution of the populations in each compartment is modeled through a set of differential equations:

$$\begin{aligned}
 \frac{dS_k(t)}{dt} &= -\frac{S_k(t)}{N_k} \frac{R_0^{(k)}}{D_I} I_k(t) \\
 \frac{dE_k(t)}{dt} &= -\frac{S_k(t)}{N_k} \frac{R_0^{(k)}}{D_I} I_k(t) - \frac{E_k(t)}{D_E} \\
 \frac{dI_k(t)}{dt} &= \frac{E_k(t)}{D_E} - \frac{I_k(t)}{D_I}
 \end{aligned} \tag{2}$$

where:

- $S_k(t)$ ,  $E_k(t)$ ,  $I_k(t)$ , and  $R_k(t)$  are the number of susceptible, latent, infectious, and removed individuals at time  $t$  in group  $k$ ;
- $D_E$  and  $D_I$  are the mean latent (assumed to be the same as incubation) and infectious period (equal to the serial interval minus the mean latent period);
- $R_0^{(k)}$  is the basic reproductive number in population  $k$ .

The main issue with this deterministic set of equations lies in the fact that it does not provide any natural uncertainty quantification for estimates of  $R_0$ , nor any Maximum Likelihood Estimate formulation of the  $R_0$  coefficient — and thus, provides no natural notion of uncertainty, especially given that all the parameters that are fed into these equations are (informed) guesses, that come

with their own level of uncertainties. Some studies have introduced stochastic components in SEIR models, for instance in the study of Ebola [9]. However, it is not standard to take into account the heterogeneity of the basic reproductive numbers  $R_0$  — thus potentially hindering the realism of their predictive scenario.

**Model.** Here, we build upon a simplification of the compartmental model. The heterogeneity of  $R_0$  is modeled using a Bayesian hierarchical workflow. Our model is based on the non-parametric model by Fraser [6], also used for estimating  $R_0$  in Cori et al [2]. A version of this model was implemented in the R-package `EarlyR` [11], which has been used in recent studies[13] to infer COVID 19's  $R_0$ . Instead of explicitly modeling the exposed and infected periods separately —based solely on the number of new infections— this model foregoes the modeling of latent cases and relies solely on inferring the number of new cases from previous observations using an “infectivity profile” [2]. In this setting, each infected case is expected to contaminate on average of  $R_0$  patients (by definition) — but the distribution of this number of new infections is given by a probability distribution which only depends on the time  $s$  elapsed since infection: one could indeed imagine a patient becoming increasingly contagious over the first few days of the infection as the viral load builds up, and decreasingly so after the peak of the illness. This infectious profile is typically modeled as a Gamma distribution. Since this quantity is generally unknown and hard to estimate from available data, Cori et al [2] propose the use of the parameters of the serial interval (for which we typically have much more substantial observational data and means of estimation) as a good proxy. The only drawback of this model compared to the SEIR compartmental one is that the exponential growth phase is only valid for the first stages of the epidemic (on shorter timelines), and will thus not yield informative scenarios in longer time horizons (several years) — but it does provide a valid estimate of  $R_0$  that we can then plug in as parameter in any deterministic model. Our goal is to assess the toll of hospital load that a rapidly propagating pandemic can induce. As such, we emphasize that we focus on **short-term estimation**, and the study of the uncertainty for time frames of a few weeks, rather than months — since it could also be argued that due to the dynamic nature of the problem and rapidly changing policies, scenarios for months or years ahead are extremely hard to devise.

Moreover, in our setting, we focus solely on the uncertainty on  $R$ , which we assume to have a

distribution over space and time. That is, we assume the parameters of this serial interval to have been correctly estimated and thus, the coefficients  $w_s$  to be known. We discuss in the appendix how to add some uncertainty to these parameters.

We call  $X$  the number of incident (new infectious) cases each day. The incidence on day  $t$  conditioned on the previous incidences can be modeled by a Poisson distribution of the form:

$$\forall t \leq T, \quad X_t \sim \text{Poisson}(R_0 \sum_{s=1}^{t-1} w_s X_{t-s}) \quad (*)$$

where  $w_s = \mathbb{P}[\Gamma_{\alpha,\beta} \in (s, s+1)]$ .

Here, we assume a hierarchical structure following Eq. 1 for  $R$ , which takes into account the inherent spatial variability and decomposes it as the product of the transmissibility  $\tau$ , the daily contact  $\bar{c}_g$  and the duration of individual infections  $D_i$  — which we assume to be known. We propose to assume here the transmissibility to be common across all groups, and the rate of contact  $\bar{c}_g$  to be group-specific, as it is intrinsically tied to locally varying parameters (age demographics, social and cultural habits and current local policies), etc. This decomposition also provides a convenient way to model the effect of the measures deployed by governments to try to control the spread, which effectively targets diminishing the reproductive number  $R$  by reducing the daily contact rate  $\bar{c}$ . Here, we propose to model the transmission rate as being drawn from a Beta distribution, while we assume a Gamma distribution for the  $\bar{c}_g$ s. The generating mechanism is summarized in the plate model provided in Figure 4.

One of the issues with this model is the one of identifiability: the product  $\bar{c}\tau$  is invariant by rescaling of the two factors. To get rid of this identifiability issue, we propose to adopt a similar strategy as in classical logistic regression examples: we fix the first group's daily contact rate  $\bar{c}_1$  to a fixed value — we pick it here to be 1. Intuitively, this assumes that any infected person in population 1 to be in average in contact with one susceptible person per day. All other values of  $\bar{c}$  can thus be understood as relative measures with respect to this benchmark group — thus a  $\bar{c}_2$  with value 2 would indicate that, on a daily basis, an infected individual in population 2 has twice as many contacts in the susceptible group than in population 1. This benchmark value could be either an arbitrary benchmark value (which should allow the potential  $R$  to vary within reasonable ranges),

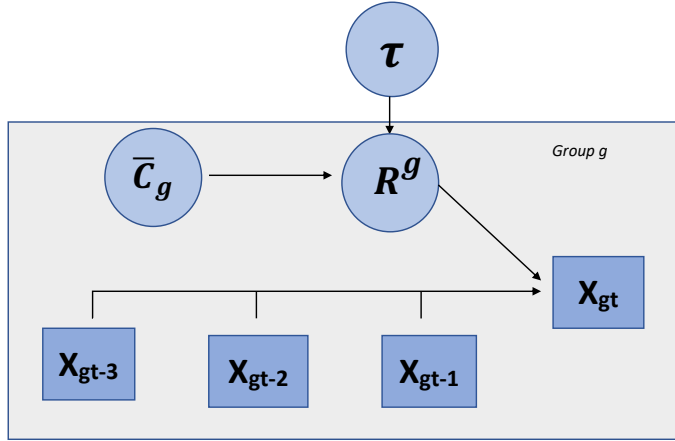


Figure 4: Plate model

or an informed measure of social interactions — for instance, a daily contact of one person per day might seem like an appropriate value for a population in complete lockdown, such as seen in Wuhan as of January 22<sup>nd</sup>.

The model is summarized below:

$$\begin{aligned}
 \forall t \leq T, \forall g \leq G, \quad X_{t,g} &\sim \text{Poisson}(R^{(g)} \sum_{s=1}^{t-1} w_s X_{g,t-s}) \\
 \forall g = 2 \cdots G, \quad \bar{c}_g &\sim \Gamma(2, 1) \\
 \tau &\sim \beta(1, 39) \\
 R^{(g)} &= \bar{c}_g \tau D_I
 \end{aligned} \tag{3}$$

The full random-effect version of this model follows the same framework, except, instead of considering a fixed  $R^{(g)}$ , at each time step, the effective reproductive rate  $R_t^{(g)}$  is sampled from a gamma distribution:

$$R_t^{(g)} \sim \Gamma(R_0^{(g)} * 10, 10)$$

We provide in Appendix B a formal comparison of this hierarchical framework with the results provided by the methodology detailed in Cori et al [2] when  $R_0$  is fitted on the whole data, or respectively independently on each group.

**Model Fitting and Validation.** To fit this hierarchical model, we use the `RStan` programming suite[1]. This uses Hamiltonian Monte Carlo to generate samples and estimate the different parameters of the model. We use a total of 8 chains, with 5,000 warmup iterations and 1,000 sampling steps. All the associated code and data are provided on Github<sup>2</sup>. Appendix A provides a set of synthetic experiments that we use to benchmark the accuracy of our method.

## Analysis of the COVID-19 Data

We now deploy our approach on the 2020 COVID-19 pandemic dataset openly provided by the Center for Systems Science and Engineering at Johns Hopkins University<sup>3</sup>. The goal of this subsection is to deploy our approach to the analysis of large geographical groups, where we expect social and environmental factors to vary substantially — and thus, the  $R_0$  to exhibit a high amount of variance. In most countries outside of China, the past few weeks have seen the critical surge of the pandemic. In contrast, current reports have shown that the epidemic is slowing down in mainland China. We thus propose to focus on the analysis of the period from February 9th to March 17th (where the epidemic has steadily grown in the world without — for the most part — massive social distancing or public policy measures). We use the next five days (March 18th to 22nd) for validation .

We consider a total of 19 distinct geographical groups, spread around the world in order to gauge the amount of variability shown in the reproductive number  $R$ :

- the six countries reporting the highest numbers for the epidemic in Europe (Italy, Spain, France, Germany, the United Kingdom and Switzerland),
- seven groups in Asia (Hong Kong, the Chinese provinces of Guizhou and Hubei, Singapore, Thailand as well as Japan and South Korea),
- Iran,

---

<sup>2</sup>[https://github.com/donname/heterogeneity\\_R0](https://github.com/donname/heterogeneity_R0)

<sup>3</sup>Data openly available: <https://github.com/CSSEGISandData/COVID-19>

- and finally, the United States as a whole, as well as the states of California, Washington and New York.

These groups are highlighted on the map in Figure 5b.

For most of these groups, as shown in the plots in Figure 6, the epidemic still seems to be in its early stages and growing exponentially. To contrast it with later stages in the epidemic, we also fit the model separately to the data from the provinces of Hubei for first 36 days after the beginning of the quarantine (starting January 22<sup>nd</sup>, 2020) — a group that we refer to as “Hubei 0”. This group is taken to be our reference group (we assume that in this case, the number of daily contacts is 1).

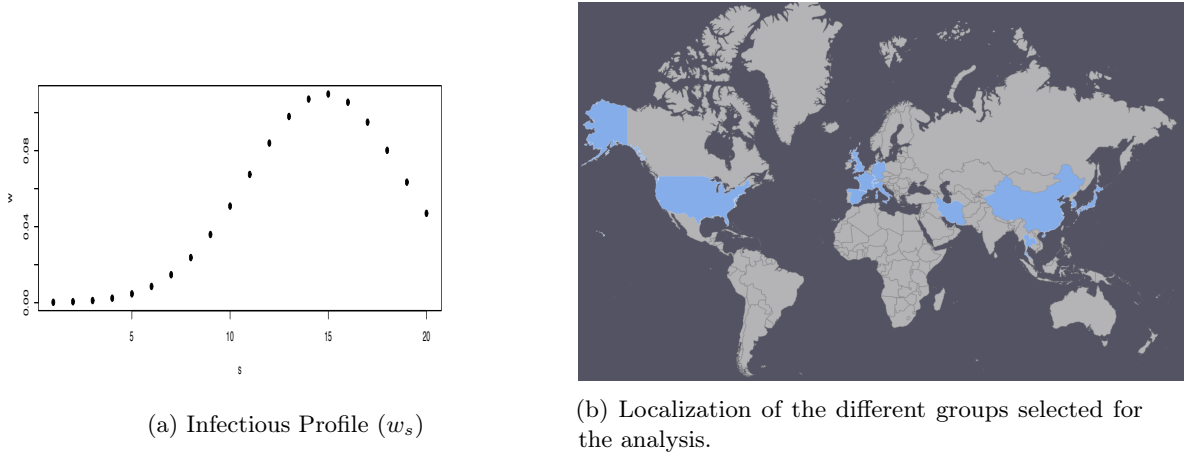


Figure 5: Parameters (infectious profile and selected groups) chosen for the analysis.

### Preliminary Exploratory Data Analysis.

The plots shown in Figure 6 show the time series for a few of our selected epidemic groups, and highlight the need to make our analysis more robust. Indeed, the exact date of the onset of the epidemic in each group is uncertain, as is shown on those plots by the fact that the different countries are currently at different stages of the epidemic. In particular, we note the substantial lag of the United States with respect to Europe — though the sudden spike in number of reported cases seems to indicate an under-reporting of previous cases, potentially due to lack of testing. To account for this under-reporting of the number of early cases, we introduce a random variable  $\mu_0^{(g)}$  modeling these phantom, unreported cases. We also observe the existence of what seems to be (a) different times of

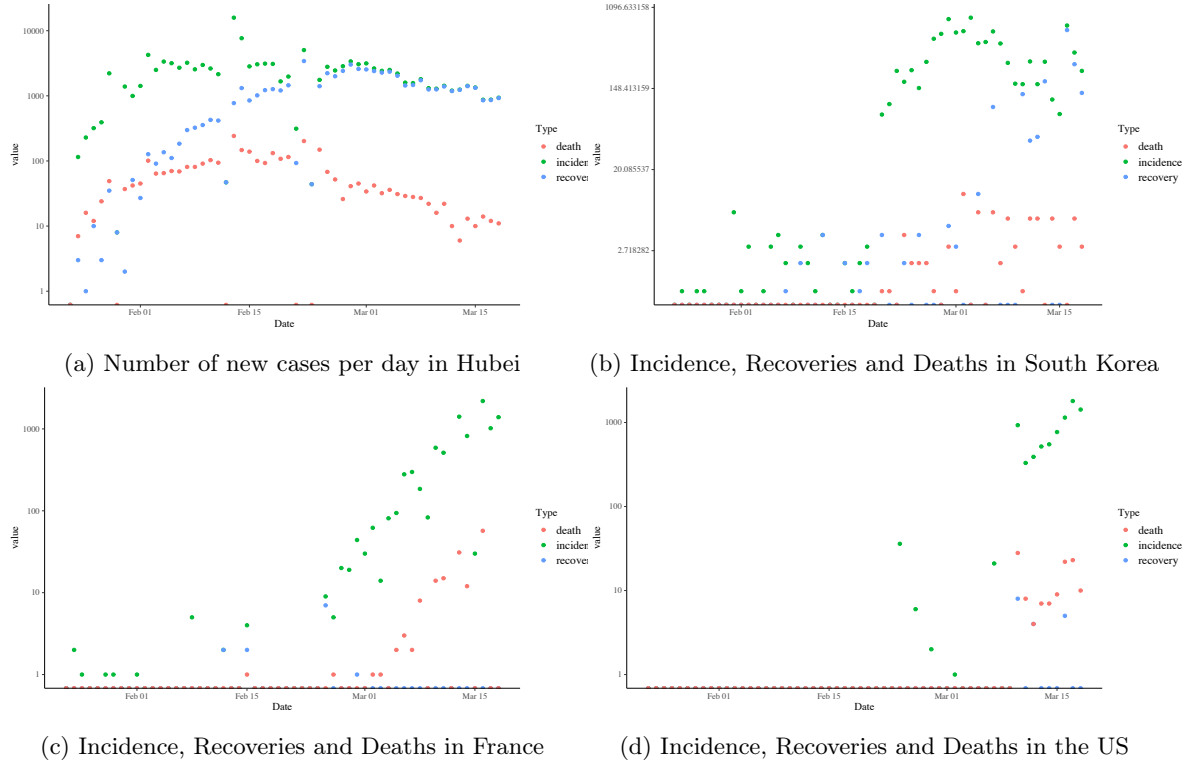


Figure 6: Incidence data for some of our selected groups

onset of the epidemic across the various groups and (b) erroneous reporting— as the increments in the number of deaths are sometimes negative. We correct the latter by thresholding the increments at 0 — that is, we assume that these negative increments are due to an error in the reporting. For the first, we propose a slight adaptation of the Poisson Model proposed in the previous subsection. To model the different onsets of the epidemics, we introduce switching dynamics through a variable  $\theta_g \in [1\dots36]$ , indicating the time of the onset of the exponential growth in the corresponding group.

We use a variance stabilizing transform: instead of directly modeling Poisson counts, we perform an Anscombe transform of the data:

$$Y_{gt} = 2\sqrt{X_{gt} + \frac{3}{8}}$$

which has the effect of ensuring:

$$Y_{gt} \approx \mathcal{N}\left(2\sqrt{R^{(g)} \sum_{s=1}^K w_s X_{g,t-s}} + \frac{3}{8}, 1\right)$$

The generative model is summarized below and in Fig. 7:

$$\begin{aligned} \forall \theta_g \leq t \leq T, \forall g \leq G, \quad Y_{t,g} &\sim \mathcal{N}\left(2\sqrt{R^{(g)} \sum_{s=1}^K w_s X_{t-s,g}} + \frac{3}{8}, 1\right) \\ \forall g = 2 \cdots G, \quad \bar{c}_g &\sim \Gamma(2, 1) \\ \tau &\sim \beta(1, 29) \\ \forall k, \mu_{g,k}^{(0)} &\sim \text{Gamma}(50, 1) \\ R^{(g)} &= \bar{c}_g \tau D_I \\ \theta_g &\sim \text{Unif}(1, 36) \end{aligned} \tag{4}$$

where  $X_{g,-k} = \mu_{g,k}^{(0)}$ ,  $\forall k \in [1 \cdots K]$

Let us now consider the problem of choosing the inherent parameters of the model – that is, satisfactory values for  $w_s$  and  $D_I$ . We use an infectivity profile following a normal distribution with parameters  $\mu = 5.2$ , and standard deviation  $sd = 3.7$ , as reported in [5]. Indeed, in this study, the authors show that the serial interval for COVID-19 is actually closer to a normal distribution, rather than the gamma distribution that is traditionally used in such cases. Recent studies have also shown that viral shedding could last up to 20 days. We thus take  $w$  to be a 20 dimensional vector, and  $D_I = 20$ . Figure 5a shows the distribution of the values of the coefficients of  $w_s$ .

**Spatial Random-Effects Model: Fitting.** As for the synthetic experiments, we fit the model in Eq. 4 using `Rstan` [1], 8 chains with 5,000 warmup iterations and 1,000 sampling steps. Figures 8 and 9 show the posterior credible intervals for the daily contact rates, transmissibility, as well as each group’s spatial reproductive number  $R_g$  itself. As a first sanity check to the performance of the model, we compare the values of the recovered  $R$  for Hubei 0 and 1 – two different stages of the epidemic in Hubei, with a tightening of the lockdown. It is interesting and reassuring to see in Figure

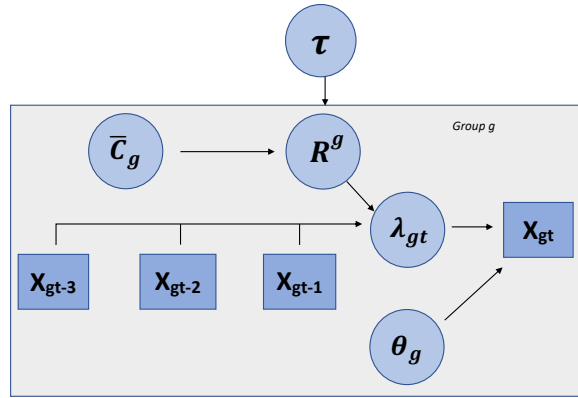


Figure 7: Plate model for the real data

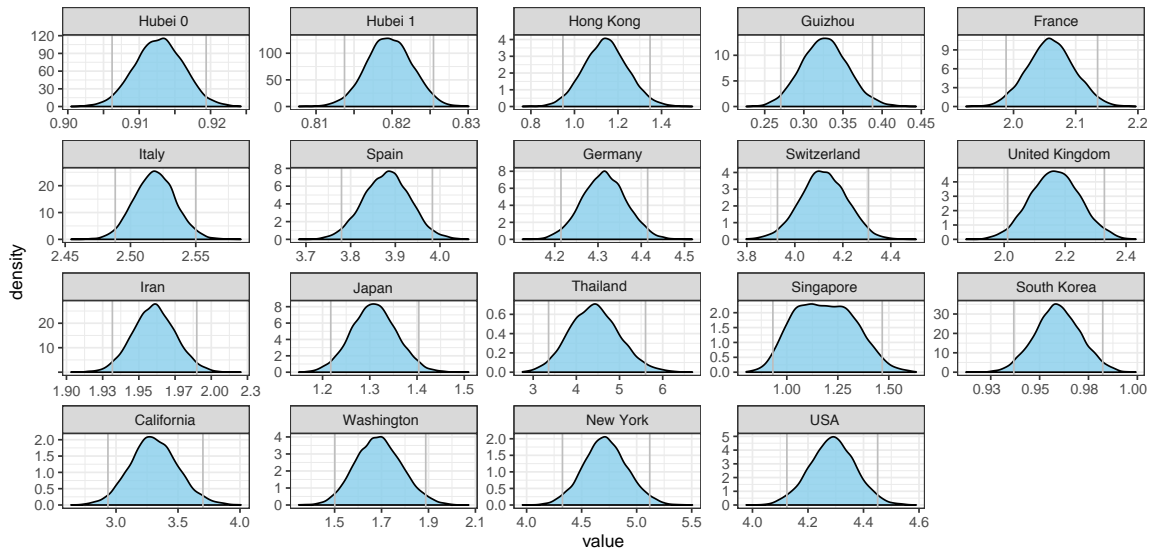


Figure 8: Distribution of the recovered spatial reproductive numbers  $R$  for the spatial Random-Effects Model.

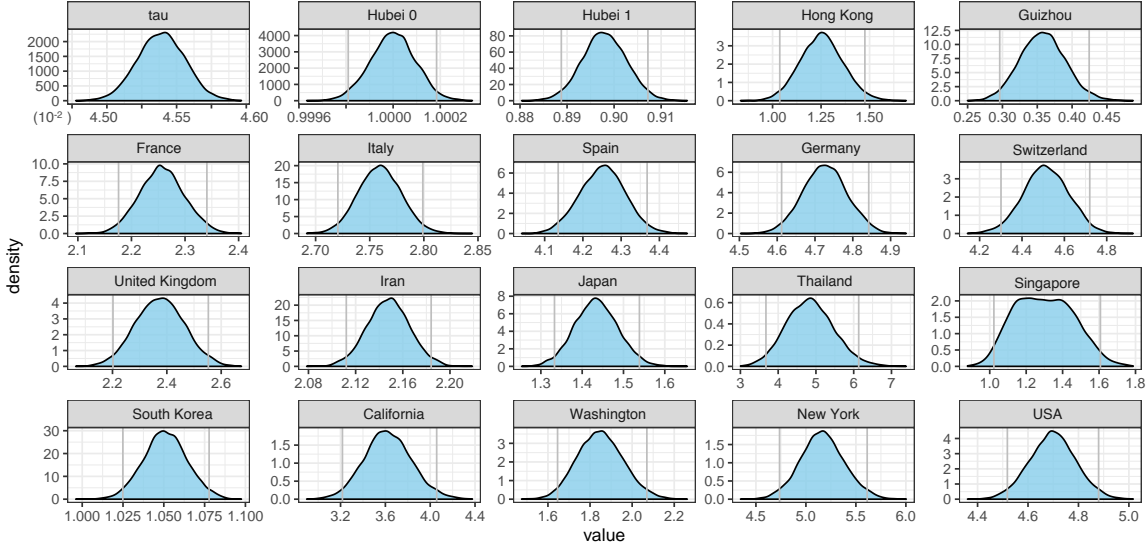


Figure 9: Transmissibility  $\tau$  and the recovered daily contact rates  $\bar{c}_g$  for the spatial Random-Effects Model.

8 that the reproductive number for Hubei does seem to have gone down, from a value of roughly 0.91 in the first days of the quarantine to 0.82 over the past 36 days — whether this decrease is due to the even tighter lockdown, or the decrease in the susceptible population, the order between these two coefficients is in the order we'd expect . Moreover, these values recovered by our model are consistent with both numbers that have been found in other studies [13, 12], as well as aligned with the  $R_0$  recovered by using the `earlyR` [11] programming suite (see (see Fig.11b, 11f,12d) — yielding in most cases similar predictions, as shown by the overlapping green (Bayesian) and pink (`earlyR`) confidence intervals. This serves as a benchmark test to our model: the Bayesian model that we use here is consistent with other statistical methods for estimating the  $R_0$ . Again, our purpose here is not to “beat” established methods, but to focus on the problem of uncertainty quantification. While in some cases, the Bayesian framework seems to be more amenable to missing and/or incomplete data (Fig.11g), our method is by no ways a substitution for this software. Rather, it provides a more amenable framework for the analysis of the variability in the predictions, and we base the following discussion on the credible intervals that our Bayesian framework provides.

**Spatial Random-Effect Model: Discussion.** Looking at the results, we note substantial hetero-

geneity in the reproductive numbers associated to the different states in America, as the reported reproductive number  $R$  varies from 3.5 in California to 1.8 in Washington — thus highlighting the importance of tailoring the estimation of the reproductive number  $R$  to a given population. The reported between-group variance is substantial compared to the within-group variance, thus emphasizing the need to adapt the estimation of the  $R_0$  to a given geographical group. This thus begs the question: in today’s general discussion about the epidemics, which  $R_0$  is actually used? Indeed, the spatial heterogeneity alone severely impacts the accuracy of the reported incident cases. This is in particular reflected in Table 1, which shows the prediction performance associated to predicting the evolution of the disease using group-specific coefficients fitted using our Bayesian framework and **earlyR**, contrasted against the predictions spanned from using the  $R_0$  computed on the aggregated dataset. For the Bayesian method, we compare predictions that make use of the spatial heterogeneity of the method, against a set of predictions based on the fixed average group value, and a third set that uses the fixed mean  $R_0$  over all groups to make the predictions. In each case, the  $R_0$  was fitted on 36 days of data (starting on February 9th), and performance evaluated on the time span from March 18th to March 22nd. We focus on the comparison of the three following metrics: (a) the length of the confidence interval provided by the method (in terms of the number of reported cases), (b) the coverage (that is, the percentage of times the observed value in the test data is contained in the interval provided by the model) and (c) the accuracy, expressed as the average difference between the predicted mean value and the actual observation. In particular, the error between the average predicted values and the actual observations using a group-specific  $R_0$  is 30% lower than the one obtained using an average  $R_0$  over the aggregated data (for both the Bayesian model and the **earlyR** estimates). We also note that the group-specific  $R_0$  obtained through our Bayesian procedure exhibits similar accuracy to the one inferred using **earlyR** (which do not benefit from the hierarchy), while yielding larger confidence intervals and substantially better coverage.

Moreover, we observe a significant variability in the confidence intervals associated to each of these  $R$ s. For instance, the width of the confidence interval for the reproductive number in Spain is roughly of length 0.2, while it is two or three times as big in other groups (e.g, California, Switzerland). This local variability thus also needs to be taken into account when running predictive scenarios, since this uncertainty is then exponentially reverberated in downstream predictive scenarios.

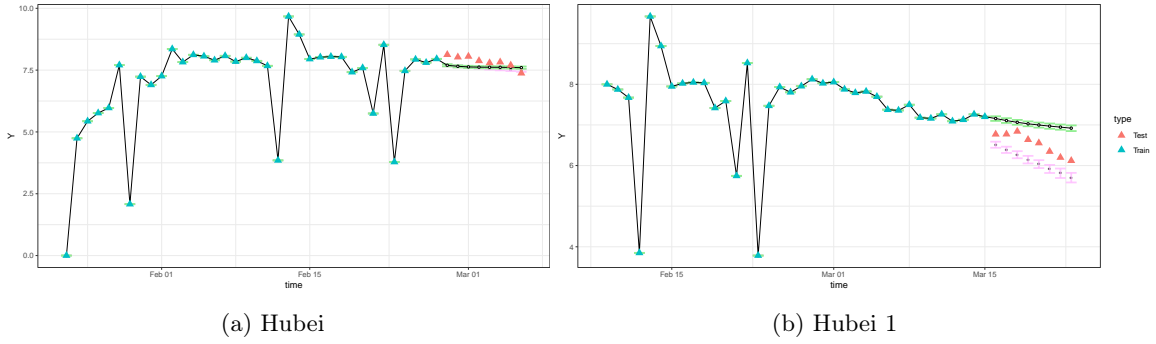


**Figure 10: Spatial Random-Effects Model.** Predictions (with confidence intervals) for Hubei 0 (first days of the quarantine) and Hubei 1 (last 36 days).  $Y$  values are plotted on the log scale. Green confidence intervals are the one recovered by our Bayesian method, and in pink through the **projection** R-package. The blue circles show the observations used for training, and the red triangles are observations from the past six days that we use as validation.

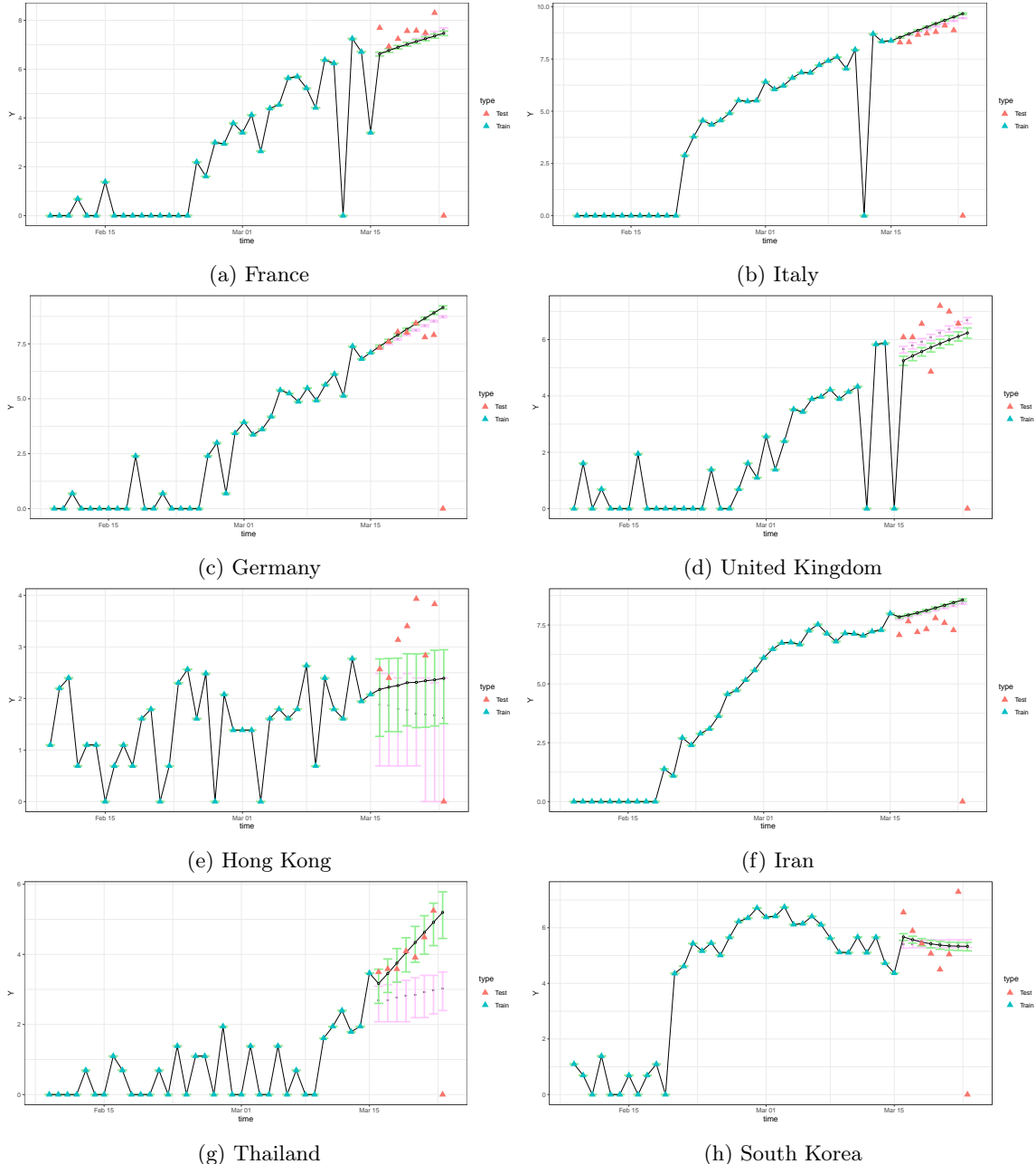


Figure 11: **Spatial Random-Effects Model.** Predictions on the log-scale for a few countries. Training observations shown by the blue circles, validation data by the red triangles. Green confidence intervals are the ones recovered by our Bayesian method, and in pink through the `projection` package.

Method	Length CI	Percentage coverage	Mean Error
Bayesian Method	214	63.9	861
Bayesian Method (Fixed, average group $R$ )	137	63.2	861
Bayesian Method (Overall average $R$ )	139	59.4	1227
EarlyR (Fitted per group)	159	51.9	769
EarlyR (Overall aggregated $R_0$ )	73	21.1	1034

Table 1: **Spatial Random-Effects Model:** Comparison of performances of the different prediction (over 5 days). For the Bayesian method, we compare predictions that make full use of the spatial heterogeneity of the method (1st row), vs one that uses the fixed average group value (2nd row), and a third that uses the mean  $R_0$  over all groups (3rd row) to make the predictions. We compare these results to the coefficients obtained using `earlyR` fitted independently on each cluster (4th row) or over the aggregated data (5th row).

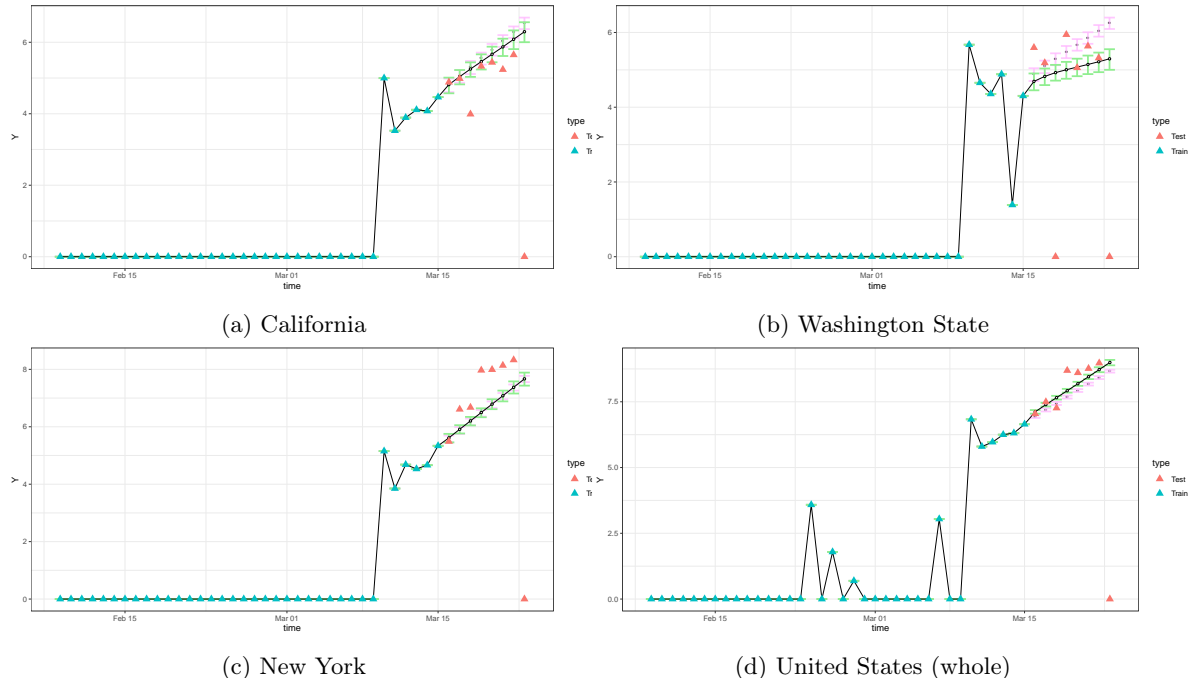


Figure 12: **Spatial Random-Effects Model.** Predictions (log-scale) for the United States. Green confidence intervals are the one recovered by our Bayesian method, and in pink through the projection R-package.

Table 1 and the predictive plots in Figures 11 and 12 thus emphasize the importance of tailoring the  $R$  coefficient to the given group: note in particular the variability in the length of the confidence intervals from group to group.

These results thus highlight the need to integrate the heterogeneity of the spatial distribution of

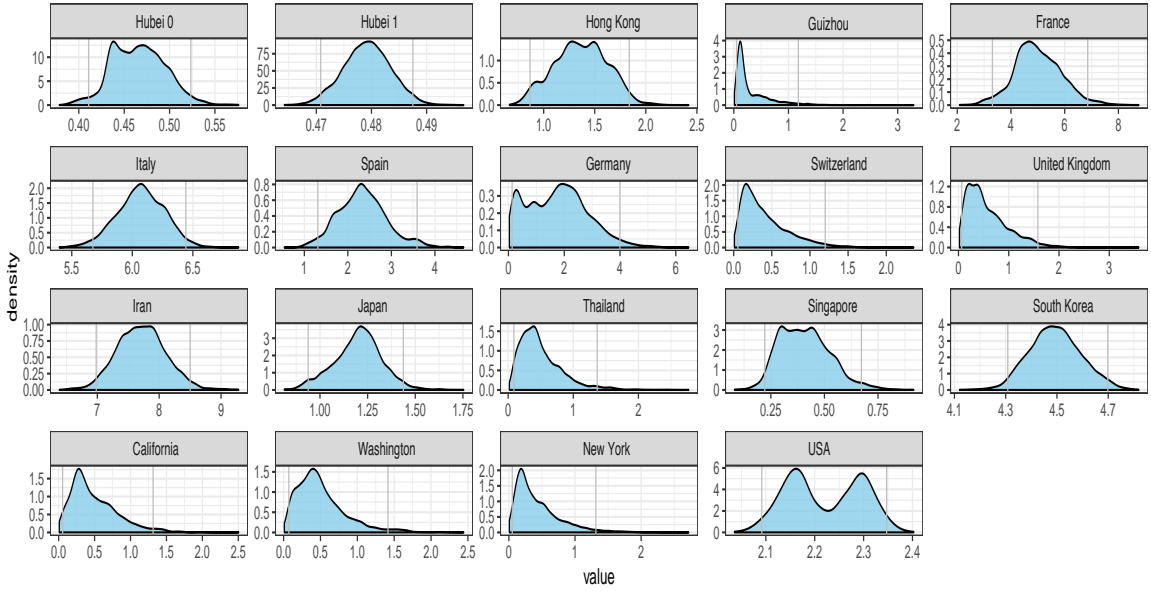


Figure 13: Distribution of the recovered spatial reproductive numbers  $R$  for the random effects modelling for the full Random-Effects model — fitted on 36 consecutive days from February 9th to March 17th

$R$  in the model to yield informative models. Note however that this model is only valid for the first weeks of the epidemic, as this assumes an exponential growth model.

**Full Random-Effects Model: Fitting.** We now assess the impact of adding further variability in the group  $R^{(g)}$  reproductive coefficient, modeling it itself as a random variable which is re-sampled at every time step. Similarly to the previous setting, we fit the random-effect model using `RStan` with 8 chains, 5,000 warmup iterations and 1,000 sampling steps. We discard two of the chains that had not mixed with the others.

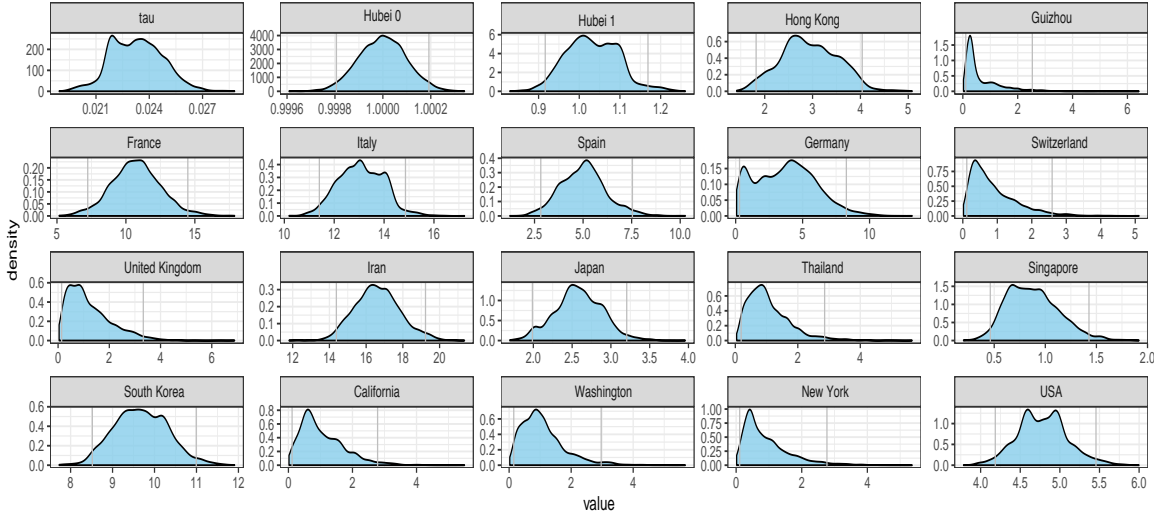


Figure 14: Transmissibility  $\tau$  and the average recovered daily contact rates  $\bar{c}_g$  for the full Random-Effects model.

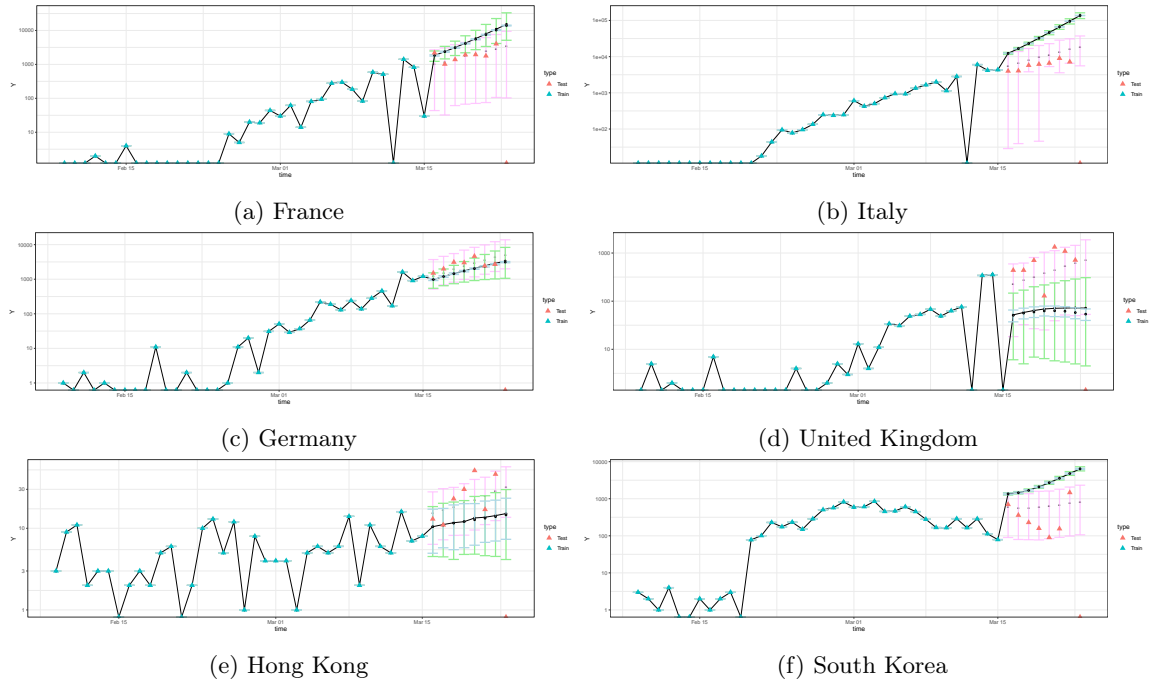


Figure 15: **Full Random-Effects Model.** Predictions using random effects on the log-scale for a few countries (training observations shown with the blue rounds, validation data displayed through the red triangles). Pink confidence intervals are the ones recovered by our Bayesian complete random-effect model (new  $R_i^{(g)}$  for every time step in each trajectory), green are confidence intervals obtained assuming  $R^{(g)}$  is random, but constant through time (one  $R^{(g)}$  per trajectory), and in blue, the ones assuming that  $R^{(g)}$  is fixed and equal to its mean recovered value

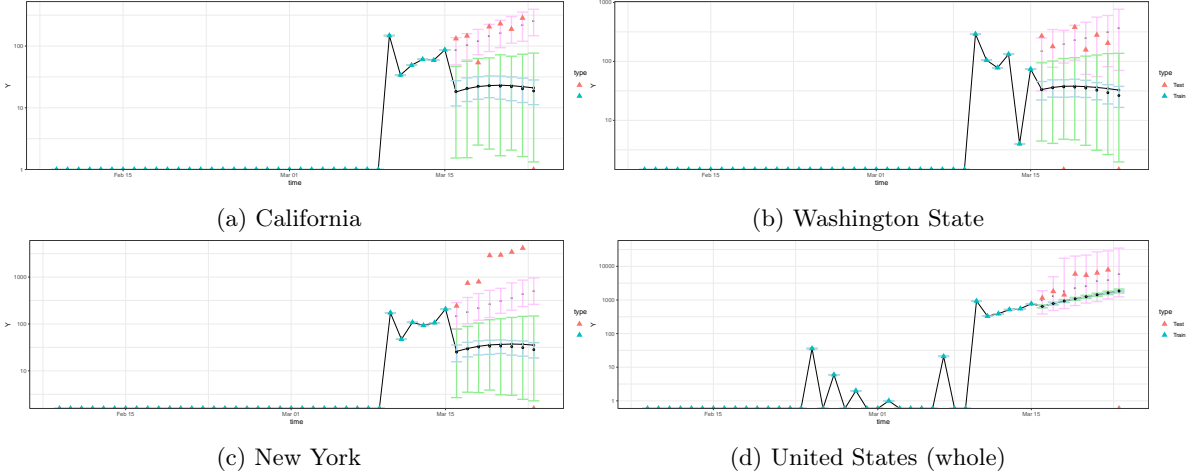


Figure 16: **Full Random-Effects Model.** Predictions (log-scale) for the USA. Training observations shown with the blue round, validation data displayed through the red triangles. Pink confidence intervals are the ones recovered by our Bayesian complete random-effect model (new  $R_i^{(g)}$  for every time step in each trajectory), green are confidence intervals obtained assuming  $R_i^{(g)}$  is random, but constant through time (one  $R_i^{(g)}$  per trajectory), and in blue, the ones assuming that  $R_i^{(g)}$  is fixed and equal to its mean recovered value.

**Discussion: Full Random-Effects Model.** The results for the full random-effects model are displayed in Figures 13 and 14. Note that the shapes of the distribution of the  $R_g$  are radically different than in the Spatial Random-Effect Model. In particular, the credible intervals are substantially larger. We also note that the distribution for the  $R_0$  corresponding to the United States exhibits a slight bimodal behavior: this could be due to the heterogeneity of the United States data, which consists of the raw counts of the epidemic aggregated over different states at various stages of the epidemic.

Figures 15 and 16 illustrate the advantage of adding temporal variability to the  $R_0$ . Indeed, for this fitted model, the confidence intervals for the  $R$  are much larger than in the Spatial Random-Effects model. The predictions are, in average, more accurate using the fully random model rather than using the average group  $R_0$  (the average group value fitted in this version of the model). For instance, using the average  $R_0$  recovered in this setting, the average difference between the mean trajectory and the actual observations is around 5,000. The error is however cut by 40% by using the fully Bayesian model. The confidence intervals — albeit far greater for the fully random model than for the the spatial random-effects model — nonetheless provide a better coverage of the actual observations (87% for the pink fully random credible intervals, to be compared against 49% for the green partially

random ones, and 40% for the blue ones corresponding to the constant  $R_0$ ), thus pointing to a more realistic quantification of the uncertainty.

**Partial Conclusion: Effect of the Variability on Uncertainty Quantification.** From our simulations and experiments on real data, it seems that taking into account the complete variability of the  $R_0$  is important to plan ahead for worst-case scenarios. Indeed, while the mean error is twice as big for the full random-effects model compared to the spatial one and the average-case scenarios thus seem to be better predicted by the less variable model, the true difference lies in the extreme cases. In particular, the coverage by the provided credible intervals is less optimal for the spatial random-effects model compared to the fully Bayesian one (64% vs 87%). In either of these models, the predictions obtained by holding  $R_0$  constant, aggregated over the whole data, yields confidence intervals that are too narrow, and predictions that are completely off. Additional temporal and spatial variability seem therefore necessary to draw a more complete portrait of the outcomes of the epidemic (and especially the extreme), as well as to correctly quantify its uncertainty.

### 3 Evaluating the impact of adding heterogeneity in predictive scenarios.

The second stage of our analysis is to use our fitted model for the heterogeneous  $R$  and local group demographics to predict the impact of different strategies on the outcome of the epidemic. Indeed, policy makers are currently faced with the difficult task of implementing efficient policies to limit the spread of the virus, while arbitrating between societal and economical costs. An inspection of the decomposition of the reproductive number provided in Eq. 1 exhibits why a policy geared towards a lowering of the daily contact rate  $\bar{c}$  should efficiently limit the spread of the virus. The goal of this section is thus to quantify the effect of governmental measures on the “flattening of the curve”. Again, we emphasize that our study does not aspire to provide state-of-the-art prediction models, but rather to assess how informative our exponential growth model truly is when used in the context of drawing predictive scenarios under such huge uncertainty. As such, we use our fitted reproductive number to generate new predictions for the next 200 days. The results that are presented in this

section are inferred from running 800 simulations.

Note that we do not want to assume here that a given policy can manage to bring the  $R_0$  to a given value (e.g. 1) – in other words, that the effect of the policy is absolute. Rather, because different countries have different governmental structures, population (and household) dynamics, it seems more sensible to talk about a spectrum of social distancing measures and to discuss the effect of a policy in relative terms. We thus consider policies that divide the daily contact rate by a certain factor, rather than in absolute value. On an aside note, one could envision assessing a given policy's effective slashing of the contact rate using population census data (for the structure of the household) as well as general mobility data. Historical data could indeed be used estimate baseline contact rates, while current mobility data would reflect the effective contact rate associated to a given policy. Thus, we characterize policies not as categorical variables (e.g, "Total Freedom", "Shelter-In-Place", "Lockdown", "R=1", and so on), but as continuous variables (i.e, reduction of  $\bar{c}$  to 20% of its original values, etc.).

Since one of the main issues when handling the pandemic consists in the access to healthcare, we use the predicted epidemics trajectories to model hospital bed occupancy. Studies have indeed shown that hospitals are able to deliver the best care up to 85% of capacity — threshold after which the quality of the care decreases. This can lead to a potential increase in fatality rates for COVID-19, as well as unwanted additional comorbidities, as people suffering from other ailments do not receive proper access to treatment. Thus, this part will focus on modeling the number of beds (general hospitalized and Intensive Care Unit (ICU)) required by patients suffering from COVID-19 at any moment in time (rather than the incident cases themselves), as well as the cumulative death toll.

The model that we adopt here is the following. For each day:

1. We generate the number of new incident cases based on the Bayesian model detailed and fitted in the previous section.
2. We then generate the number of people among these incidence cases that will require hospitalization. This number is generated by a binomial distribution, with a hospitalization rate that is contingent on the geographic localization and takes into account the age demographic layout

of each cluster:

$$\pi_{\text{Hosp}}^{(g)} \sim 0.01 * \Gamma(\alpha_g^T \pi_{\alpha}^{\text{Hosp}}, 1)$$

where  $\alpha_g$  is the proportion of each age group in location  $g$  (divided in 4 groups: from “0-19” years-old, “20-54”, “54-65”, and “65+”), and  $\pi_{\alpha}$  is the hospitalization rate per group (expressed in percentages, and assumed to be universal across all contagion groups).

3. Once the number of newly hospitalized people has been selected, we choose among them using a binomial distribution the people directly admitted into an Intensive Care Unit (ICU). The parameter for the binomial is also contingent on the demographics:

$$\pi_{\text{ICU}|\text{Hosp}}^{(g)} \sim \frac{0.01 * \Gamma(\alpha_g^T \pi_{\alpha}^{\text{ICU}}, 1)}{\pi_{\text{Hosp}}^{(g)}}$$

where  $\pi_{\alpha}^{\text{ICU}}$  is the ICU rate per group (also expressed in percentages, and assumed to be universal across all contagion groups).

4. Finally, the fatalities are chosen among the people placed in the ICU, and sampled from a binomial distribution with probability:

$$\pi_{\text{death}|\text{ICU}}^{(g)} \sim \frac{0.01 * \Gamma(\alpha_g^T \pi_{\alpha}^{\text{death}}, 1)}{\pi_{\text{ICU}}^{(g)}}$$

5. All the hospitalizations, ICU and number of deaths being selected, we assign a time of death of each patient and of departure from the hospital/ICU by sampling from a normal distribution, whose mean and standard deviation have been selected based on numbers based on recent studies.

The scenarios are thus sampled as follows:

$$\begin{aligned}
\tau &\sim \text{Posterior}(\tau) \\
\forall g, \quad \bar{c}_g &\sim \text{Posterior}(\bar{c}_g) \\
X_{t,g} &\sim \frac{1}{2} \left( \mathcal{N} \left( 2 \sqrt{R_0 \sum_{s=1}^K w_s X_{t-s} + \frac{3}{8}}, 1 \right) \right)^2 - \frac{3}{8} \\
\pi_{\text{Hosp}}^{(g)} &\sim 0.01 * \Gamma(\alpha_g^T \pi_{\alpha}^{\text{Hosp}}, 1) \\
\pi_{\text{ICU}|\text{Hosp}}^{(g)} &\sim \frac{0.01 * \Gamma(\alpha_g^T \pi_{\alpha}^{\text{ICU}}, 1)}{\pi_{\text{Hosp}}^{(g)}} \\
\pi_{\text{death}|\text{ICU}}^{(g)} &\sim \frac{0.01 * \Gamma(\alpha_g^T \pi_{\alpha}^{\text{death}}, 1)}{\pi_{\text{ICU}}^{(g)}} \tag{5} \\
\text{Hosp}_{t,g} &\sim \text{Binomial}(X_{t,g}, \pi_{\text{Hosp}}^{(g)}) \\
\text{ICU}_{t,g} &\sim \text{Binomial}(\text{Hosp}_{t,g}, \pi_{\text{ICU}|\text{Hosp}}^{(g)}) \\
\text{Deaths}_{t,g} &\sim \text{Binomial}(\text{ICU}_{t,g}, \pi_{\text{death}|\text{ICU}}^{(g)}) \\
\forall i \in [1 \dots \text{Deaths}_{t,g}], \quad T_i^{\text{Deaths}_{t,g}} &\sim N(\mu_d, \sigma_d) \\
\forall i \in [1 \dots \text{ICU}_{t,g}] \quad T_i^{\text{ICU}_{t,g}} &\sim N(\mu_{ICU}, \sigma_{ICU}) \\
\forall i \in [1 \dots \text{Hosp}_{t,g}] \quad T_j^{\text{Hosp}_{t,g}} &\sim N(\mu_h, \sigma_h)
\end{aligned}$$

We emphasize again that our predictive model for the number of incident cases is based on some version of the exponential growth model. As such, it is only valid for the first stages of the epidemic but not for long-term predictions of the disease, where traditional SEIR models are typically better suited to the task. Our goal here is to assess the speed at which hospitals can be swamped with patients at the beginning of the epidemic, and to understand how the variability impacts our selection of a course of action mitigating the social and economical costs associated to a complete lockdown of a geographical region. We also want to assess the efficient of alternation-based scenarios, in which the population would remain under lockdown for  $x$  days (that is, a state of activity in which the normal number of daily contacts is divided by a factor  $y$ ), and pursue almost regular activities for the remainder of the week.

**Spatial Random-Effects Model: Discussion.** We focus on the analysis of the results for the

projected epidemic trajectories for a few of our groups. Note that the results here should be interpreted as the trajectories, based on the data obtained on March 18th, if the governments had immediately implemented a given public policy. As such, there might be a few discrepancies with the current observed numbers — but again, the focus of this paper is to assess the impact of the added variability on the uncertainty of the projected scenarios rather than on the accuracy of the scenarios themselves, so as to answer the following question: how informative truly are our predictive scenarios?

**Case Study 1: France** Panel 17 shows the evolution of hospital occupancy and death rate in France using different reproductive numbers  $R_s$  as input and using preventive measures to stall it. In particular, Panel 17(A) shows the predictive results for the number of beds occupied by COVID-19 patients, ICU units, and daily death toll for strategies using an average  $R_0$  (fitted on the aggregated data for the 19 groups that we have been considering in this paper). These have to be contrasted against the predictions we can obtain in Panel 17(B), where the group-specific  $R$  for France is used to draw the predictive scenarios. Note in particular the lack of consensus between the outputs of these scenarios: for the general mean  $R_0$ , slashing daily contacts by 60% is sufficient to obtain prevent hospitals from overflowing within the next two months. This is barely sufficient for the group-specific  $R$  (with much longer resolution horizon), and scenarios, such as alternating 3 days of lockdown with an 80% reduction in the daily contact rates with four days of business as usual is no longer sufficient to resolve the healthcare overflow. This highlights the importance of using the group-specific reproductive rate.

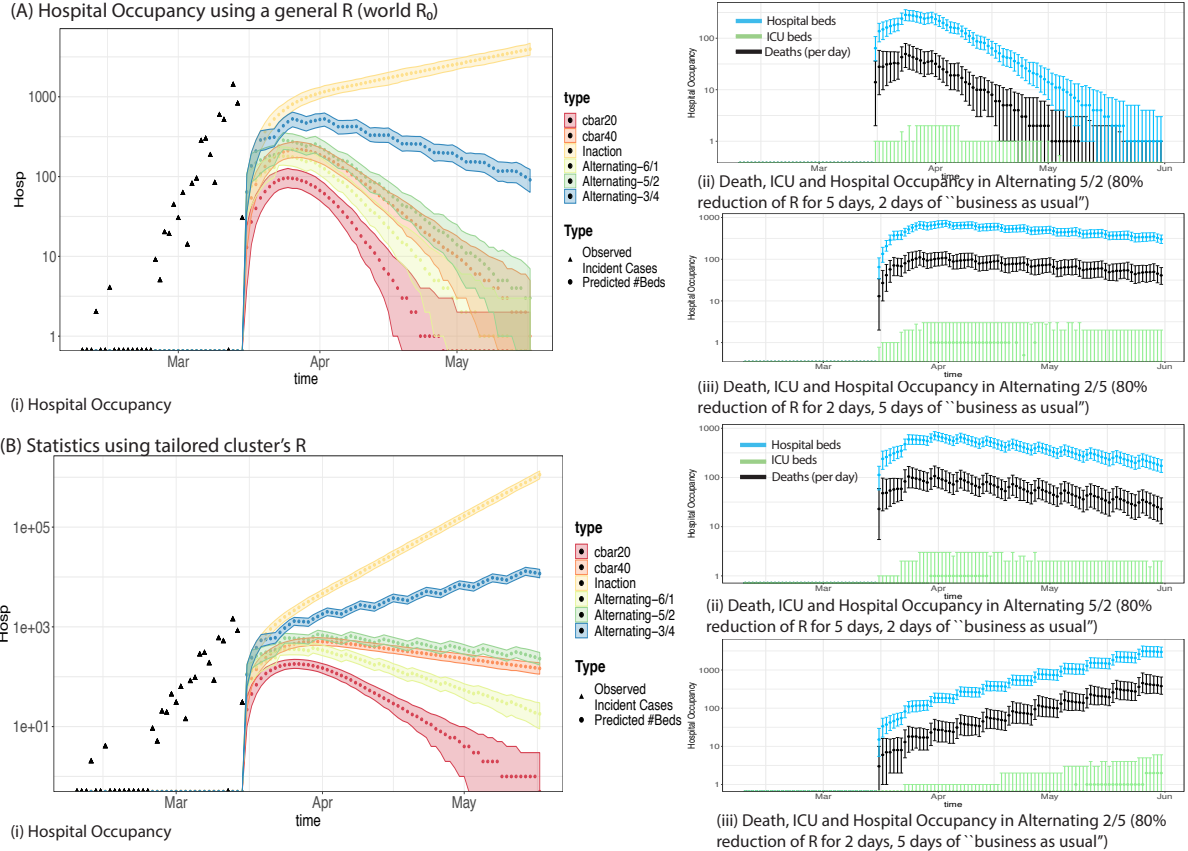


**Figure 17: Spatial Random-Effects Model: France.** Comparisons of the outcomes of the different strategies. We compare the estimated likely trajectories in terms of occupied hospital beds using various  $R$ : the group's specific and tailored Bayesian  $R$ , as well as an overall, general  $R$  estimated from the aggregated data. We note the substantial difference in the impact on the healthcare systems that the aggregation vs the spatially heterogeneous  $R$  yield.

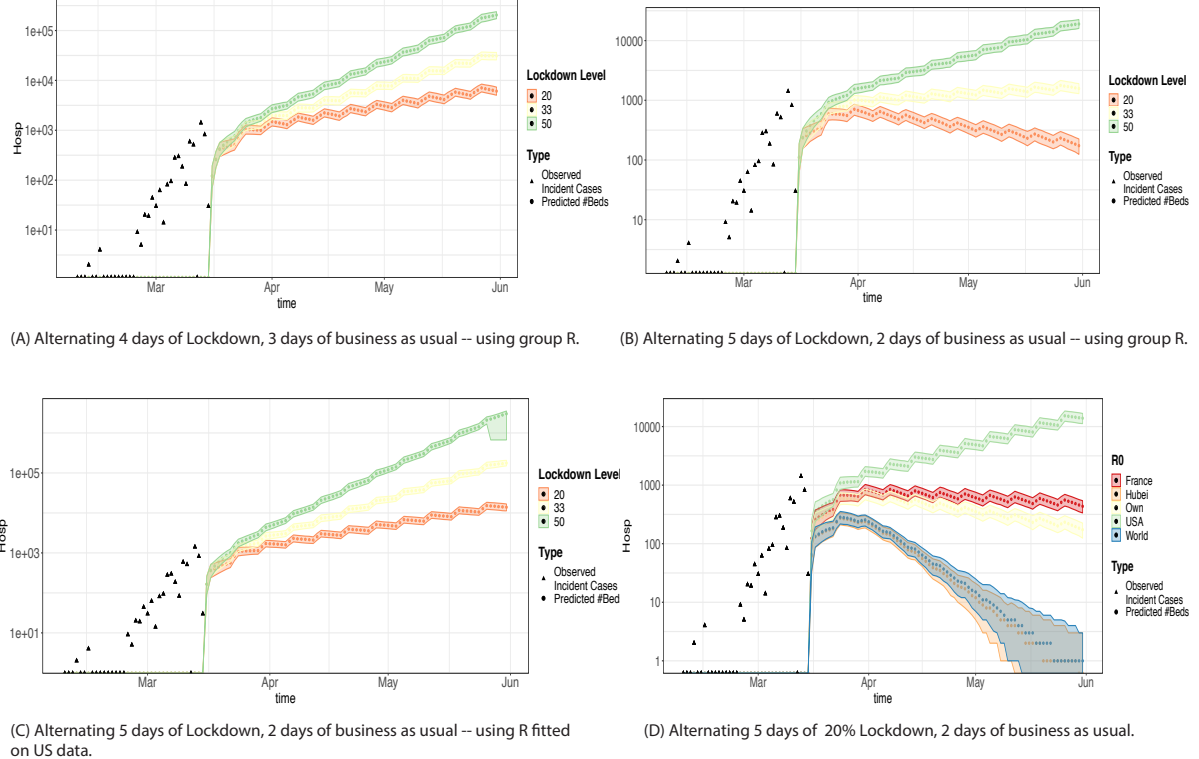


Figure 18: **Spatial Random-Effects:** France. Comparisons of the outcomes of the different strategies. We compare the estimated likely trajectories in terms of occupied hospital beds using various  $R$ : the group’s specific and tailored Bayesian  $R$ , as well as an overall, general  $R$  estimated from the aggregated data. We note the substantial difference in the impact on the healthcare systems that the aggregation vs the spatially heterogeneous  $R$  yield.

Figure 18(D) shows the hospital capacity as predicted by the different  $R_0$ s — that is, for models where the  $R_0$  is either drawn from the distribution of another country (to test for transferability), from the group-specific distribution, or is a fixed  $R_0$  estimated from the aggregated data. Not only do the scenarios vastly differ, we note that some of the alternating strategies will not be valid under an inappropriate  $R_0$ , as they will not be to contain the growth of the epidemic and the overflow of the hospital system.

**Case Study 2: The United States** We also show the same results for California (Fig. 19) and the

United States (Fig. 20). Due to the country's large  $R_0$ , the model seems to hint towards a complete saturation of the hospitals within three weeks. We also note that in this case, a slashing of  $\bar{c}$  to 40% of its original value is no longer sufficient to prevent the explosion of the hospital occupancy. Finally, the difference between the predictive scenarios for California and the United States as a whole seem to highlight the need to perform the analysis at a very fine grain level.

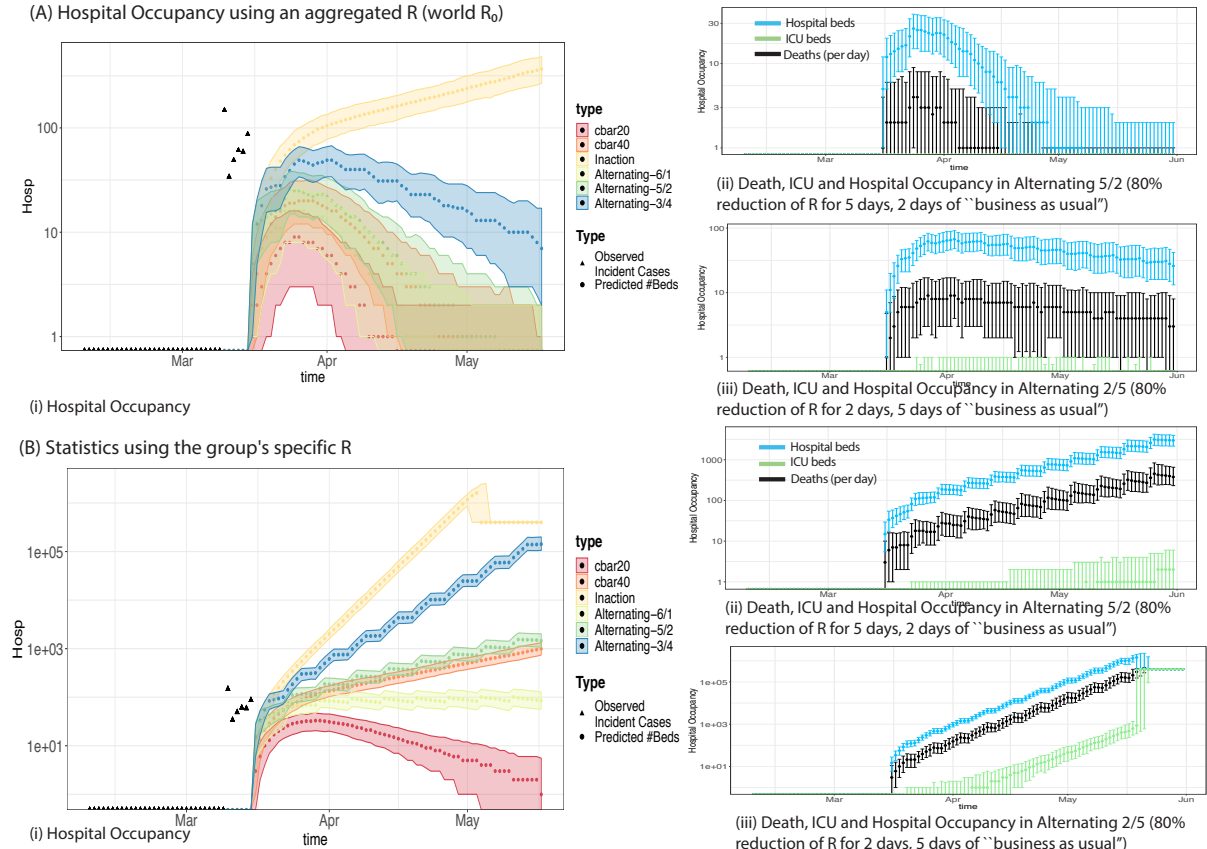


Figure 19: **Spatial Random-Effects: California.** We compare the estimated likely trajectories in terms of occupied hospital beds using various  $R$ : the group's specific and tailored Bayesian  $R$ , as well as an overall, general  $R$  estimated from the aggregated data. We note the substantial difference in the impact on the healthcare systems that the aggregation vs the spatially heterogeneous  $R$  yield.

Figure 21 shows the different scenarios produced for four different groups and comparing the effect of using different fitted values for the  $R_0$ , compared to their own. This highlights the impact of fitting the appropriate  $R_0$ , and the lack of transferability between the different clusters.

On the other hand, we note that sampling from each posterior interval for each  $R_g$  obtains similar

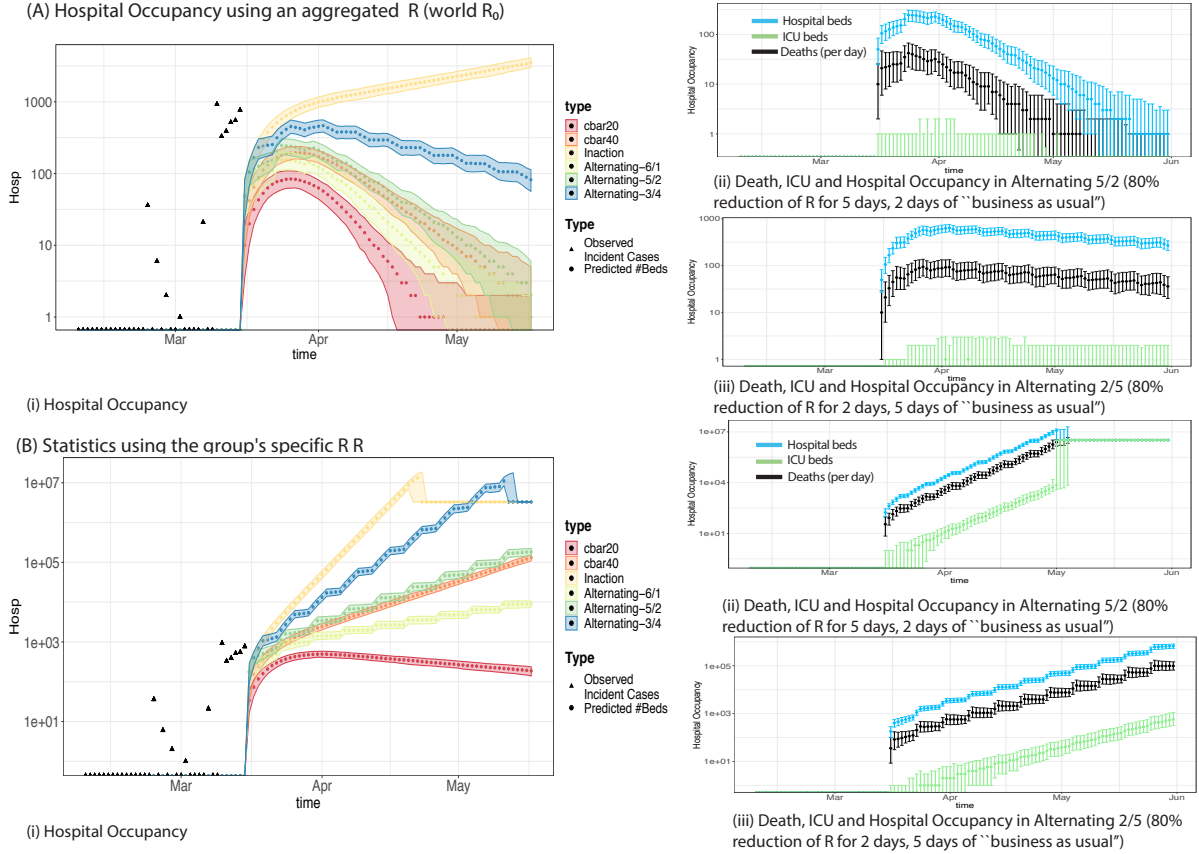


Figure 20: **Spatial Random-Effects.** United States of America

prediction bands that by running the same model using the mean  $R_g$ . Fig. 22 shows that the confidence bands for our predictions of the number of new incident cases per day are not significantly narrower than our projected scenario using the mean  $R_0$  of the distribution. This is because the confidence intervals recovered by the Bayesian model (as per Fig. 8) are for the most part quite narrow. A more realistic model for the  $R_0$  would be to model it using a heavier-tailed distribution, so as to accurately capture the existence of super-spreaders.

Our study cases and Fig. 21 thus show the impact of selecting the right  $R_0$ : not all policies yield the desired flattening of the curve, thus highlighting the need to perform a fine grain analysis of each cluster to draw informative scenarios.

**Stopping times.** To quantify the impact of the variability on the  $R_0$ , we now look at the time expected until 1% of the population is hospitalized, using different policies and  $R_0$  in the fitting

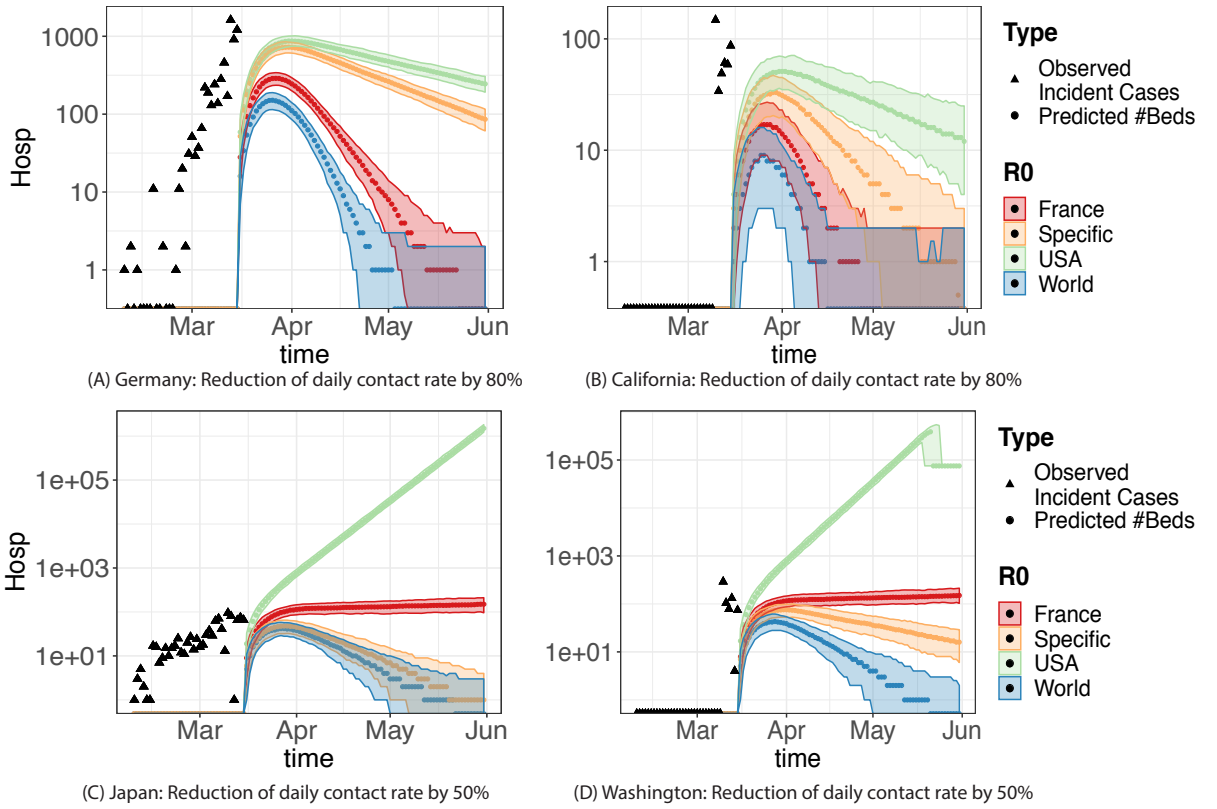


Figure 21: **Spatial Random-Effects.** Comparison Predictions: this figure further shows for four different groups the estimated impact of a given policy, using different  $R_0$ s. This shows the importance of correctly accounting for group-wise heterogeneity in the model.

procedure. Results are reported in Table 2 and in Fig. 23 and 24, which show the distribution of the stopping time obtained for a few groups. In particular, results indicate that an alternating lockdown (5 days of 50% lockdown, 2 days of business as usual) results in an explosion of the number of occupied hospital beds in 87% of the times, while it occurs with 100% of the times using other less stringent strategies. This explosion would occur roughly in 8 months (237 days — a horizon too far into the future for our model to be able to gauge it accurately, but an indicator in the efficiency of delaying this peak from 3 months to 8. On the other hand, a sustained, continuous 50% lockdown would allow the hospitalization mass to remain manageable in all cases). Similar observations follow the same line for the other groups.

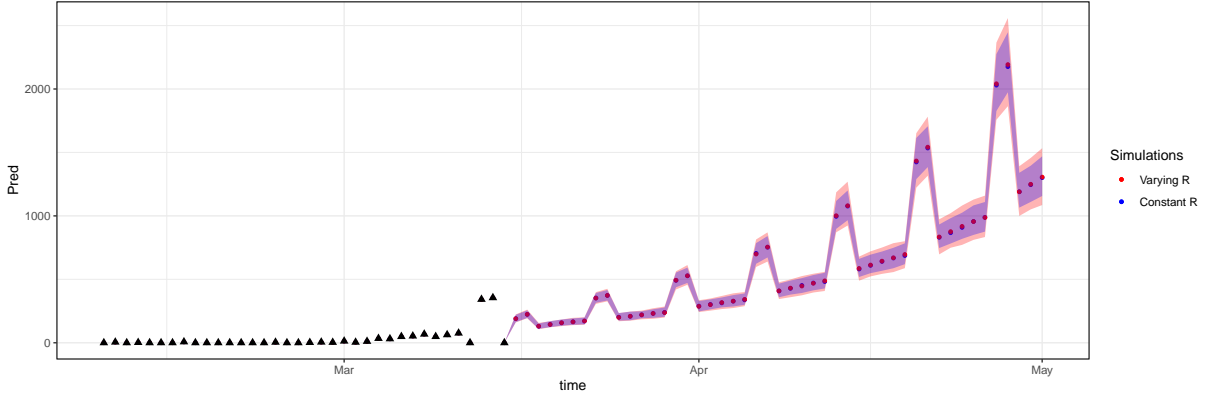
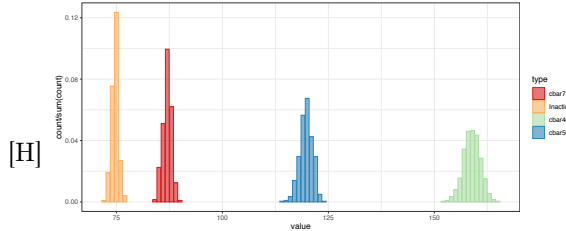


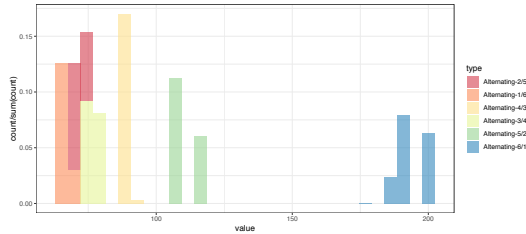
Figure 22: **Comparison Predictions: United Kingdom** for an Alternating scenario with 5 days of business as usual vs 2 days of 50% lockdown.

Stopping Time before Hospital Overflow						
Country	$R_0$ used	Strategy	Percentage	Mean $\tau$	q97.5 $\tau$	q2.25 $\tau$
France	Specific	Inaction	100	110.5	107	113
		$\bar{c}^* = 0.5\bar{c}_{France}^0$	0.00	NA	NA	NA
		Alternating 4(50%)/3	100	180	186	173
		Alternating 5(50%)/2	0	NA	NA	NA
	USA	Inaction	100	80.5	78	83
		$\bar{c}^* = 0.5\bar{c}_{France}^0$	100	106	103	109
California	Specific	Alternating 4(50%)/3	100	81	80	81
		Alternating 5(50%)/2	100	86	88	81
	USA	Inaction	100	86.1	84	88
		$\bar{c}^* = 0.20\bar{c}_{Cal}$	100	170.0	165	176
		Alternating 4(50%)/3	100	109.0	108	113
		Alternating 5(50%)/2	100	121.3	113	123
	USA	Inaction	100	75	73	77
		$\bar{c}^* = 0.5\bar{c}_{Cal}$	100	120	117	124
		Alternating 4(50%)/3	100	89	87	93
		Alternating 5(50%)/2	100	96	94	100
USA	Specific	Inaction	100	74.7	73	76
		$\bar{c}^* = 0.5\bar{c}_{US}$	100	119.9	117	123
		Alternating 4(50%)/3	100	88.4	87	92
	France	Alternating 5(50%)/2	100	95.0	94	99
		Inaction	100	125	122	128
		$\bar{c}^* = 0.50\bar{c}_{US}$	0	NA	NA	NA
		Alternating 4(50%)/3	0	NA	NA	NA
		Alternating 5(50%)/2	0	NA	NA	NA

Table 2: **Spatial Random-Effects:** Comparison of the stopping times associated to the scenarios drawn using different  $R$  (group-specific or another group's). The N/A values indicate that the stopping time has not been reached in any of our 800 simulations.



(a) USA: Time to 1% of the population under hospitalization



(b) Spain : Time to 1% of the population under hospitalization for different scenarios

Figure 23: **Spatial Random-Effects:** Histograms of the expected Time until Hospitalization Overflow for two groups.

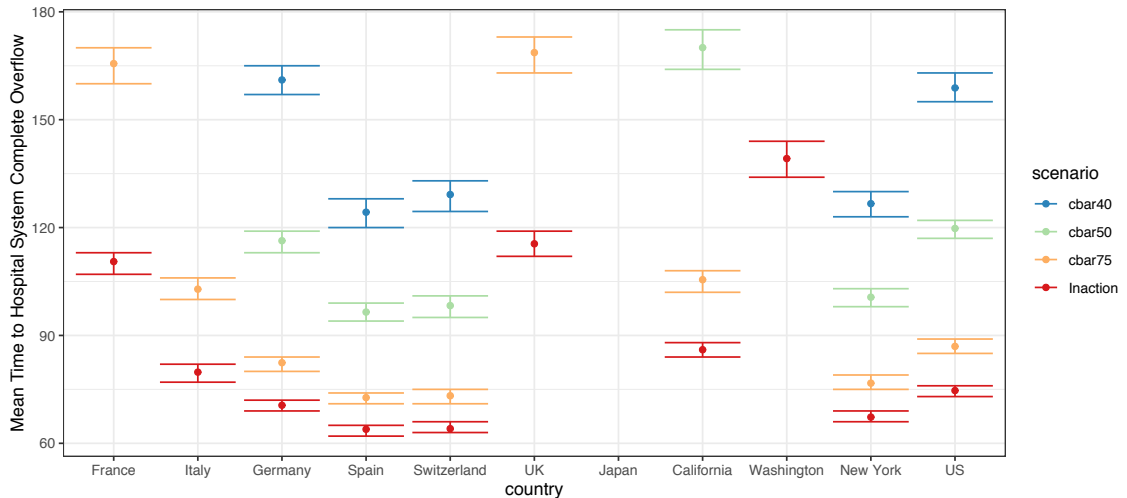


Figure 24: **Spatial Random-Effects:** Time to 1% of the population under hospitalization

**Full Random-Effects Model.** We now compare the results that we obtain using a full random-effects model, as opposed to the spatial random-effect model that we have been considering so far. As a reminder, the difference between the two is that in the full random-effects model, the  $R_0$  is

considered random and sampled from a gamma distribution at each time step. On the other hand, for the spatial random-effect model,  $R_0$  is also random, but sampled once at the beginning of the trajectory and held constant across time steps.

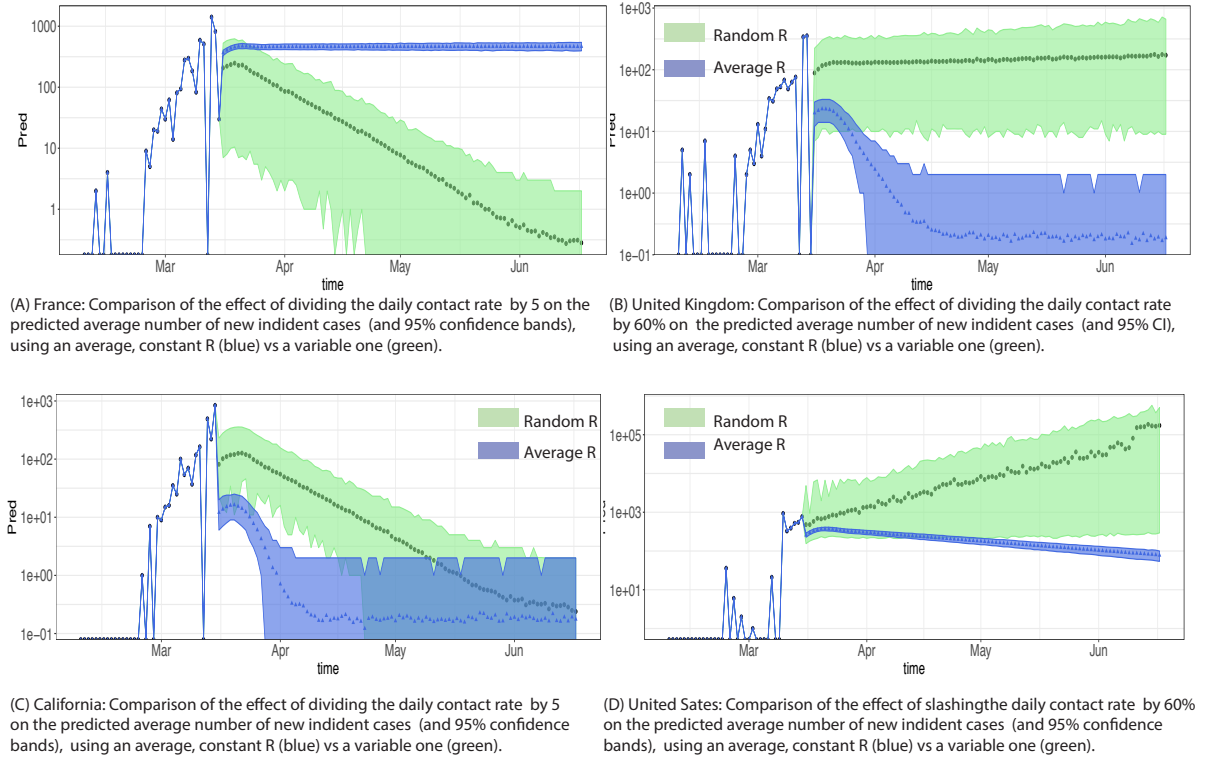


Figure 25: **Full Random-Effects:** Comparison of the Static vs Random R

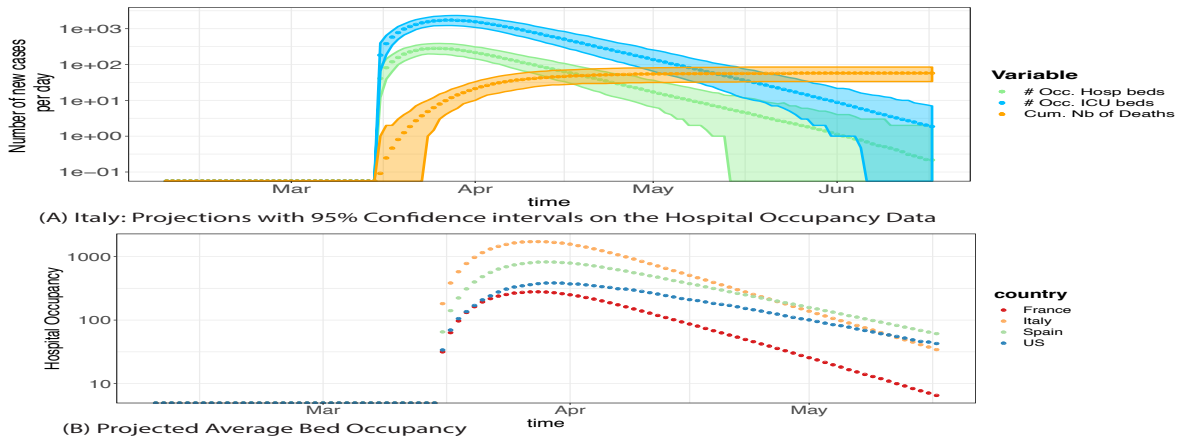


Figure 26: **Full Random-Effects:** Comparison of the projections of the occupied number of beds.

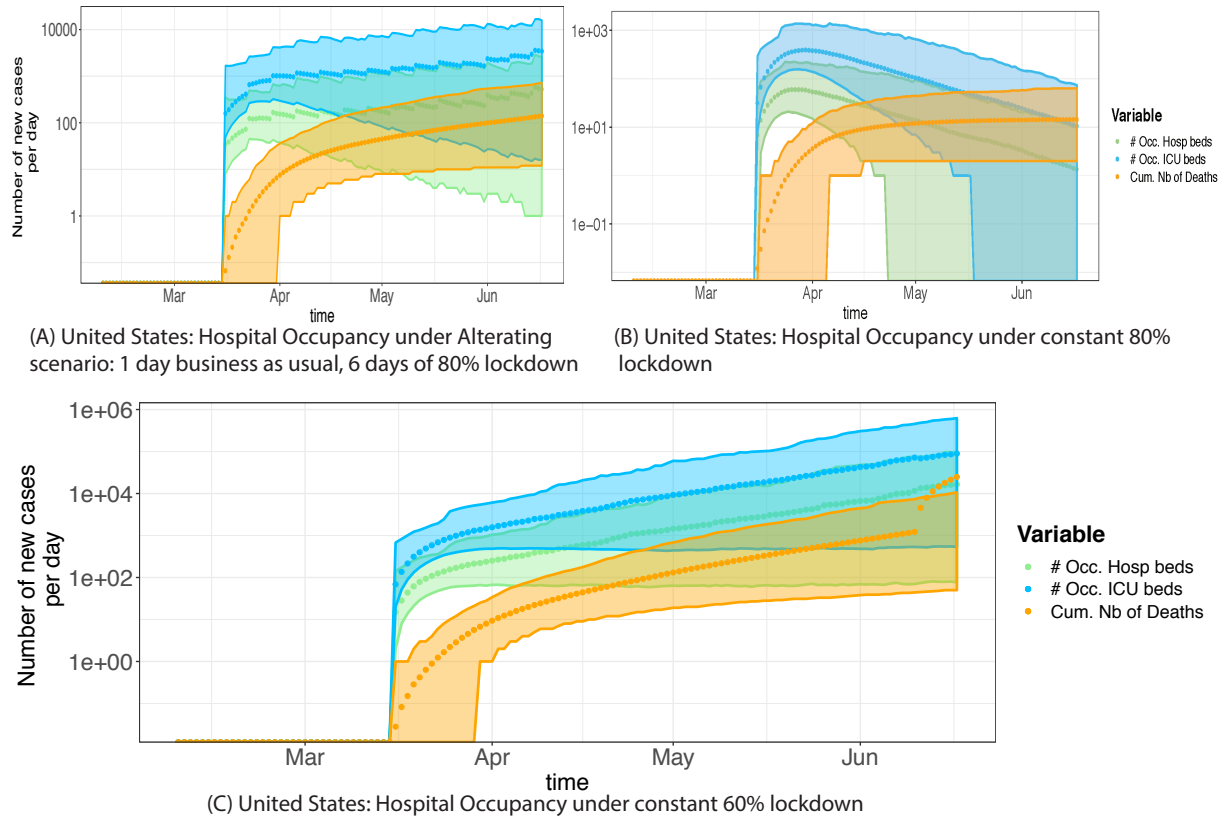


Figure 27: **Full Random-Effects:** Comparison of the projections of the occupied number of beds in the US under different social distancing scenarios.

Fig. 25 shows the comparison between the projected epidemic trajectories using a constant average mean  $R_g$  (blue dots and 95% confidence bands), vs a variable one (green dots and 95% confidence bands). We observe that the two approaches yield extremely different results. In particular, the confidence bands obtained for the average  $R_0$  are typically too narrow, and yield in Fig. 25(B-D) predictions that are more optimistic than the ones obtained with the added variability in the  $R_0$ : the resolution of the conflict seems in general much longer using the fully random  $R$  (depicted in green in Fig. 25), and can be even less likely than what is projected using the group average  $R_g$  (Fig. 25(D) ). The high difference here is due to the large credible intervals for each mean  $R_g$  that we had obtained. Thus the fixed average and fully variable scenarios rapidly diverge.

Figures 26 and 27 show more estimates of the projected average hospital occupancy across different countries. In particular, Figure 27 compares three different policies: continuous and sustained slashing of social distance by 60 and 80% (Fig 27 (C,B)), and an alternating policy of 6 days of severe lockdown (slashing of the social distance by 80%), and one of business as usual. It is interesting to see that the one day of difference between Fig.27(A) and (B) makes a significance difference: the continuous slashing is allows to prevent an overflow of the hospital with probability 1, whereas an hospital overflow happens with non-zero probability in Fig. 27(A). As already observed in the introduction, the additional variability in the full-random model extends the domain of plausible events — a crucial fact for policy-makers to correctly assess worst-case scenarios.

## 4 Conclusion

In conclusion, we have presented here an analysis targeted at assessing the level of granularity in terms of the variability necessary in the analysis to draw informative scenarios. In particular, we have shown that the modeling of this heterogeneity is crucial to correctly model extreme scenarios and characterize their uncertainty. Indeed, using a spatial and temporal random-effects model, we have shown that the added variability is necessary to (a) provide better coverage of the confidence intervals, and thus, more appropriately quantify the uncertainty associated to a certain prediction or the effect of a given policy and (b) explain rare events and understand the formation of outbreaks — which averaged models would not allow and which are nonetheless crucial elements to take into

account when weighting different scenarios.

Our analysis of the real data has also shown that the reproductive number vastly varies depending on the group considered — as such, it seems that an informative model would at least try to take into account the spatial heterogeneity, if not the full one. We emphasize again that our study does not aspire to draw predictive scenarios, but rather to understand how models and predictive scenarios are truly impacted by the choice and inherent variability of the  $R$  — and the great variability that we have imputed seems to highlight the need for a fine -grain analysis.

**Further Discussion on the Variability of  $R$ .** In our data analysis for the spatial random-effects model, we have assumed  $\bar{c}$  to follow a well-behaved  $\gamma$  distribution. We have also tried changing this to a Cauchy distribution (which has much fatter tails, and thus, could add more variability). The results we obtained with this new prior were similar to ones obtained using the Gamma distribution, thus highlighting the fact that our spatial random-effects model does not seem to be extremely sensitive to the choice of the prior.

To continue building up this work, it would be interesting to enrich our model for  $R$  with additional sources of information — thus controlling even better for the day-to-day variations exhibited in our model fit for  $R$ . In particular, this model could be improved by controlling for other environmental variables, such as the temperature, which we leave as further work.

**Disclaimer.** This model is a tool for exploring the effect of uncertainties and variation in the  $R_0$  for the virus and the effect of this variability in different types of interventions, but we do not claim to be predictive of disease dynamics for any specific populations (credit to McGee et al. for disclaimer).

## 5 Bibliography

### References

- [1] B. Carpenter, A. Gelman, M. D. Hoffman, D. Lee, B. Goodrich, M. Betancourt, M. Brubaker, J. Guo, P. Li, and A. Riddell. Stan: A probabilistic programming language. *Journal of statistical software*, 76(1),

2017.

- [2] A. Cori, N. M. Ferguson, C. Fraser, and S. Cauchemez. A new framework and software to estimate time-varying reproduction numbers during epidemics. *American journal of epidemiology*, 178(9):1505–1512, 2013.
- [3] D. J. Daley and J. Gani. *Epidemic modelling: an introduction*, volume 15. Cambridge University Press, 2001.
- [4] P. L. Delamater, E. J. Street, T. F. Leslie, Y. T. Yang, and K. H. Jacobsen. Complexity of the basic reproduction number ( $r_0$ ). *Emerging infectious diseases*, 25(1):1, 2019.
- [5] Z. Du, X. Xu, Y. Wu, L. Wang, B. Cowling, and L. Meyers. Serial interval of covid-19 among publicly reported confirmed cases. *Emerging infectious diseases*, 26(6), 2020.
- [6] C. Fraser. Estimating individual and household reproduction numbers in an emerging epidemic. *PloS one*, 2(8), 2007.
- [7] H. W. Hethcote. The mathematics of infectious diseases. *SIAM review*, 42(4):599–653, 2000.
- [8] W. O. Kermack and A. G. McKendrick. A contribution to the mathematical theory of epidemics. *Proceedings of the royal society of london. Series A, Containing papers of a mathematical and physical character*, 115(772):700–721, 1927.
- [9] P. E. Lekone and B. F. Finkenstädt. Statistical inference in a stochastic epidemic seir model with control intervention: Ebola as a case study. *Biometrics*, 62(4):1170–1177, 2006.
- [10] J. M. Read, J. R. Bridgen, D. A. Cummings, A. Ho, and C. P. Jewell. Novel coronavirus 2019-ncov: early estimation of epidemiological parameters and epidemic predictions. *medRxiv*, 2020.
- [11] P. N. Thibaut Jombart, Anne Cori. *earlyR: Estimation of Transmissibility in the Early Stages of a Disease Outbreak*. <https://CRAN.R-project.org/package=earlyR>, 2017.
- [12] J. T. Wu, K. Leung, and G. M. Leung. Nowcasting and forecasting the potential domestic and international spread of the 2019-ncov outbreak originating in wuhan, china: a modelling study. *The Lancet*, 2020.
- [13] S. Zhao, Q. Lin, J. Ran, S. S. Musa, G. Yang, W. Wang, Y. Lou, D. Gao, L. Yang, D. He, et al. Preliminary estimation of the basic reproduction number of novel coronavirus (2019-ncov) in china, from 2019 to 2020: A data-driven analysis in the early phase of the outbreak. *International Journal of Infectious Diseases*, 2020.

## A Appendix: Validation: Synthetic Experiments

Given that the problem of estimating  $R_0$  is completely unsupervised and we have no accurate way of finding proxies for the ground truth, it is necessary to run synthetic experiments to assess (a) the accuracy of the recovery of the parameters by our method given the model and (b) the sensitivity of the method to the modeling assumptions — before deploying it on real-world data.

We generate a fake epidemic time series with 10 independent outbreak groups as described in Algorithms 1. Note that Algorithm 1 generates data that follows exactly the model assumed in Eq. 4 and is thus the more amenable setting to the evaluation of  $R_0$ . Each cluster is populated with  $N_k = 5 \times 10^7$  individuals (region size), and an initial number of infected cases following a Poisson distribution with parameter  $\lambda = 10$ .

---

**Algorithm 1:** Generative Mechanism using the model by Fraser[6] and Cori et al [2].

---

**Result:** Epidemic Time series

```

Fix  $\tau = 0.1$ ,  $\bar{c}_1 = 2$ ;
Generate  $\forall g \geq 2$ ,  $\bar{c}_g \sim \Gamma(5, 1)$ ;
Fix  $K = 15$ ;
for  $g = 1$ :  $G$  do
  for  $t = 2 : T$  do
     $N_{g,t-1} \sim \text{Poisson}(R_0^{(g)} w_s^T N_{g,(t-K):t-1})$ ;
  end
end

```

---

We run the MCMC algorithm using Rstan, with 8 chains, a warmup of 10,000 iterations and a sampling phase of 1,000. All further details are provided in the Github repository along with the code.

**Comparison with current estimates.** To compare the strength of our approach, we compare it against the estimates provided by `earlyR`, which does not assume a hierarchical structure and is thus unable to leverage strength across the different clusters.

Figures 28 shows the credible densities for the  $R_0$ s obtained by our model (the ground truth values are shown by the vertical black bar), compared to ones recovered by `earlyR` (where the ground truth interval is indicated by the triangles) in Figure 29. We note that while in this "easy" case (as the

data is generated exactly by the same mechanism as per assumed by the recovery process in both methods), our method achieves 100% coverage of the  $R_0$ , and better confidence intervals than those projected by `earlyR`. The Bayesian model is thus efficient at retrieving the values for  $R_0$  for each cluster.

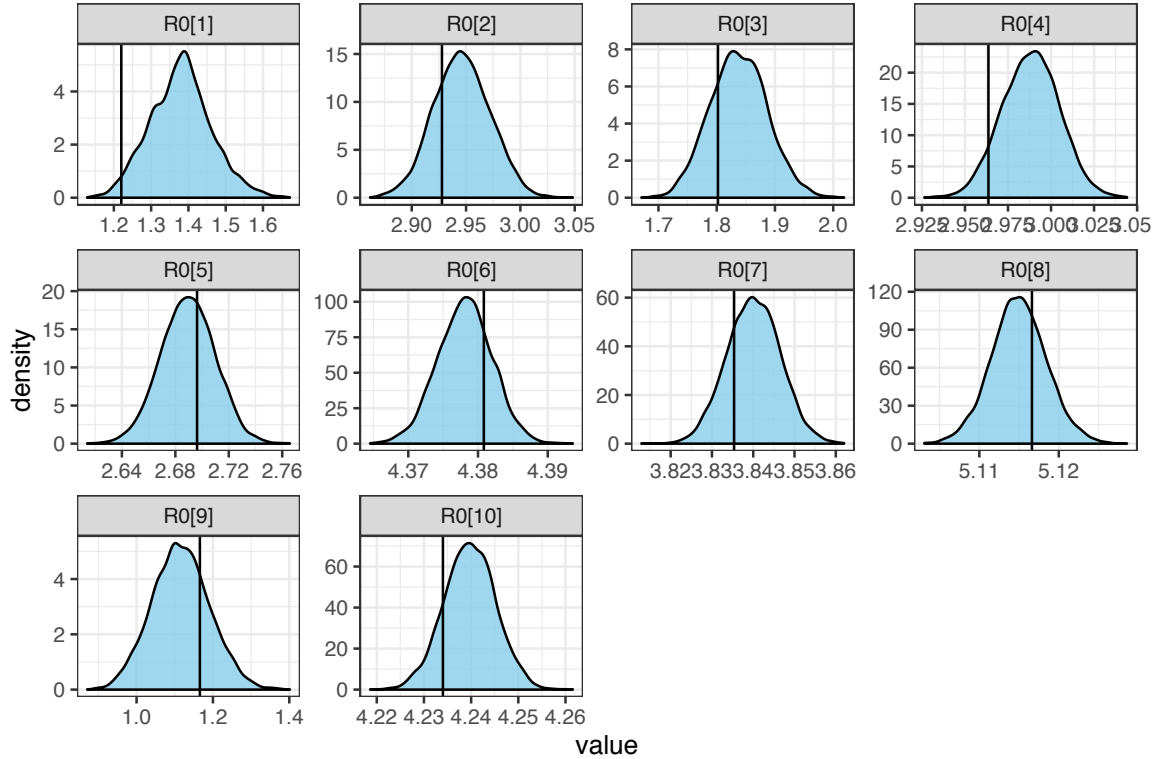


Figure 28: Recovered Credible intervals for the Fraser Model

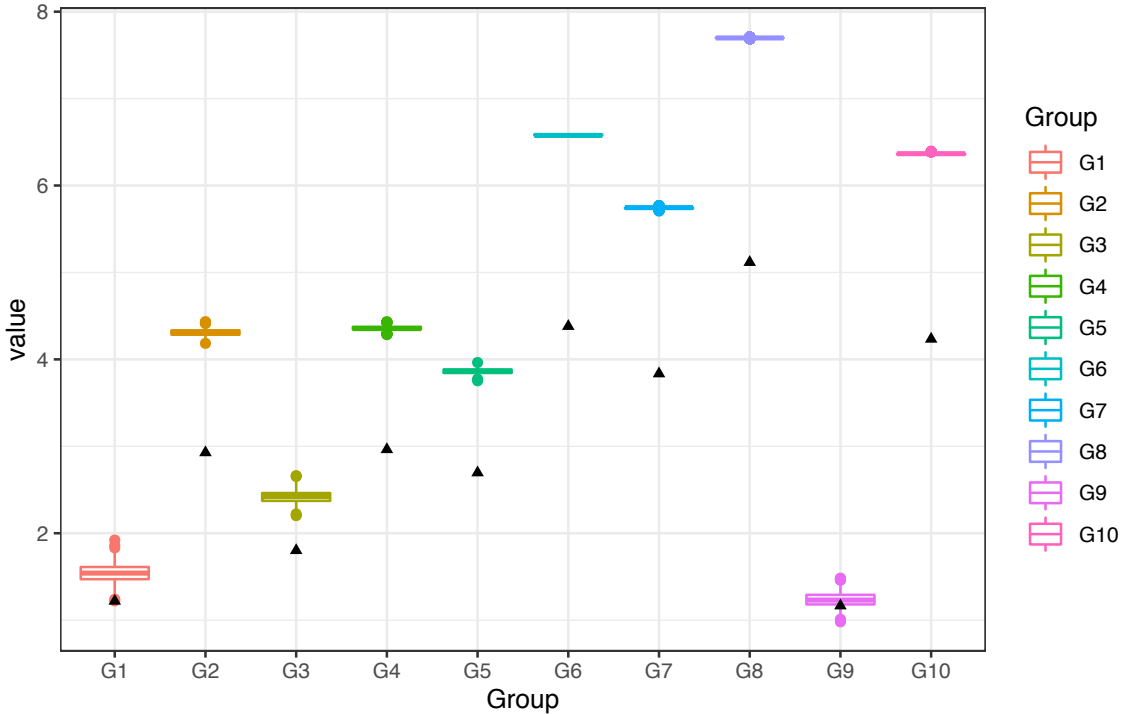


Figure 29: Boxplot of the confidence intervals obtained using the `earlyR` package using the data generated in Algorithm 1.

## B Appendix: Comparison Hierarchical Setting

**Formal Comparison of the traditional and hierarchical approaches.** We assess how much a modeling of the heterogeneity in the reproductive numbers  $R$  could make in terms of uncertainty quantification. We begin by formally writing down the log-likelihood of the model. Letting  $C$  be a constant depending only on the data (and not on the parameters of the model), the log-likelihood associated to our Poisson Model can be written as:

$$\ell(\theta) = \sum_{g=1}^G \sum_{t=1}^T \left( X_{g,t} \log(R^{(g)}) + X_{g,t} \log(\Lambda_{g,t}) - R^{(g)} \Lambda_{g,t} \right) + \text{prior on } R^{(g)} + C \quad (6)$$

with  $\Lambda_{g,t} = \sum_{s=1}^K w_s X_{g,t-s}$ . The paper by Cori et al [2] puts a Gamma prior on their estimate of  $R^{(g)}$  — to make the model more amenable to comparison, we write their reproductive number

$R = D_I \tau_0 \bar{c}$  where  $\tau_0 = 1/D_I$ , so that putting a gamma prior on  $R^{(g)}$  is equivalent to considering  $D_I$  and  $\tau_0 = 1/D_I$  fixed, and putting a gamma prior on  $\bar{c}$ . The updates at the  $b^{th}$  iteration of  $\bar{c}$  are performed independently and can be rewritten as:

$$\bar{c}^b \sim \Gamma(a + \sum_{g=1}^G \sum_{t=1}^T X_{g,t}, b + \sum_{g=1}^G \sum_{t=1}^T \sum_{s=1}^K w_s X_{t-s}) \quad (7)$$

In our case, the prior has a little more structure, since  $R_0^{(g)} = \bar{c}_g \tau$ .

$$\begin{aligned} \ell(\theta) &= \sum_{g=1}^G \sum_{t=1}^T \left( X_{g,t} (\log(\tau) + \log(c_g)) + X_t \log(\Lambda_{g,t}) - \tau c_g D_I \Lambda_{g,t} \right) \\ &\quad + \sum_{g>1} \left( (\alpha - 1) \log(c_g) - \beta c_g \right) + (\alpha_0 - 1) \log(\tau) + (\beta_0 - 1) \log(1 - \tau) \end{aligned} \quad (8)$$

In particular, the conjugate updates of our model are given by:

$$\begin{aligned} c_g^b &\sim \Gamma(\alpha + \sum_{t=1}^T X_{g,t}, \beta + D_I \tau \sum_{t=1}^T \Lambda_{g,t}) \\ \tau &\sim \beta(\alpha_0 + \sum_{g=1}^G \sum_{t=1}^T X_{g,t}, \beta_0 + D_I \sum_{t=1}^T \sum_{g=1}^G c_g \Lambda_{g,t}) \end{aligned} \quad (9)$$

where the last update in  $\tau$  follows that by assuming that the transmissibility is small, the following approximation holds:  $\log(1 - \tau) = -\tau + o(\tau)$ . Thus, by the law of total variance and linearization around  $\tau_0 = \frac{1}{D_I}$ , the variance of the  $R_0$  is:

$$\begin{aligned} \text{Var}[R_0^{(g)}] &= \mathbb{E}[\tau^2 D_I^2 \text{Var}(c_g | \tau)] + D_I^2 \text{Var}[\tau^2 \mathbb{E}[c_g | \tau]^2] \\ &= D_I^2 \mathbb{E}[\tau^2 \frac{\alpha + \sum_{t=1}^T X_{g,t}}{(\beta + D_I \tau \sum_{t=1}^T \Lambda_{g,t})^2}] + D_I^2 \text{Var}[\tau^2 \frac{(\alpha + \sum_{t=1}^T X_{g,t})^2}{(\beta + D_I \tau \sum_{t=1}^T \Lambda_{g,t})^2}] \\ &= \frac{\alpha + \sum_{t=1}^T X_{g,t}}{(\beta + D_I \sum_{t=1}^T \Lambda_{g,t})^2} + \frac{(\alpha + \sum_{t=1}^T X_{g,t})^2}{(\beta + D_I \sum_{t=1}^T \Lambda_{g,t})^2} \\ &\quad + \mathbb{E}\left[(\tau - \frac{1}{D_I})(2 \frac{1}{D_I} \frac{\beta(\alpha + \sum_{t=1}^T X_{g,t})}{(\beta + \sum_{t=1}^T \Lambda_{g,t})^3}\right] \\ &\quad + \text{Var}\left[(\tau - \frac{1}{D_I})(2 \frac{1}{D_I} \frac{\beta(\alpha + \sum_{t=1}^T X_{g,t})^2}{(\beta + \sum_{t=1}^T \Lambda_{g,t})^3}\right] \end{aligned} \quad (10)$$

This allows us to quantify the variability in the spatial reproductive number  $R$ . The bias in the variance is thus proportional to the deviation of  $\tau$  from  $\frac{1}{D_I}$ . Since we are considering exponential models (where roughly,  $R_0$  governs the slope of the exponential curve), this could lead to some substantial deviations in the predictive scenarios that are drawn.

## C Appendix: Added variability in the infectious profile

Here, we show the performance of the model when modeling  $w_s$  as a random variable. We add on top of the baseline model uncertainty in the infectious profile. The infectious profile is assumed to be sampled from an ordered dirichlet distribution, initialized with the serial interval with mean 3.96 and standard deviation 4.26, as detailed in some of the current reports. The mean length of the confidence intervals is 747.5, which is a little broader than in the case where  $w_s$  is considered to be fixed, but not substantially so.

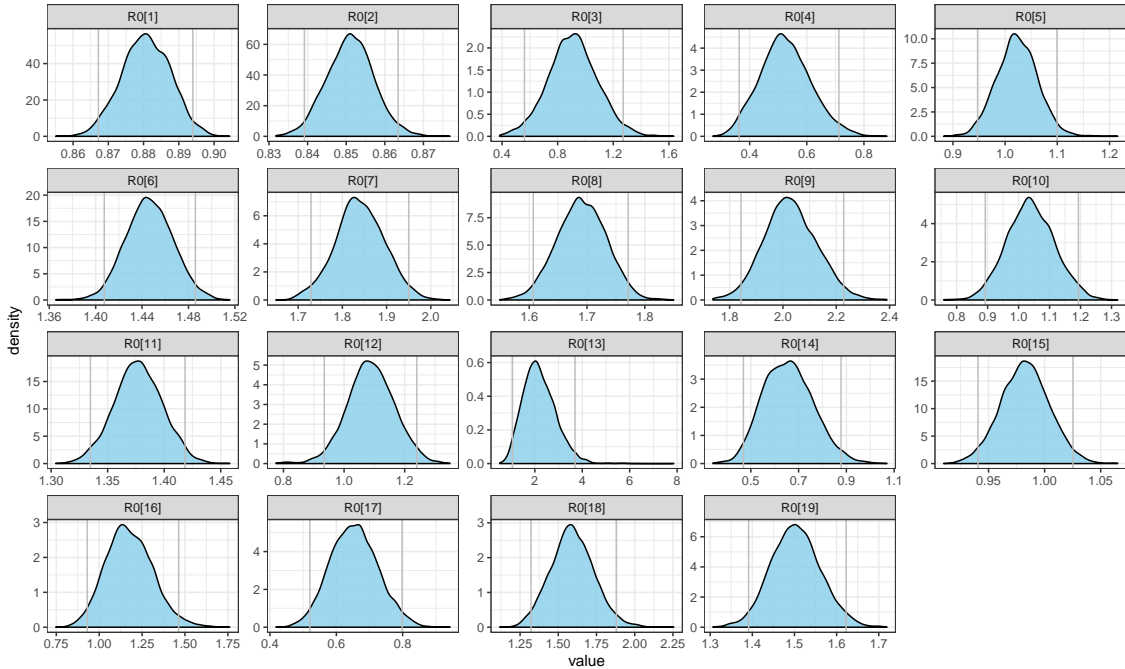


Figure 30:  $R_0$  for the spatial Random-Effects with Dirichlet estimated infectivity profile.

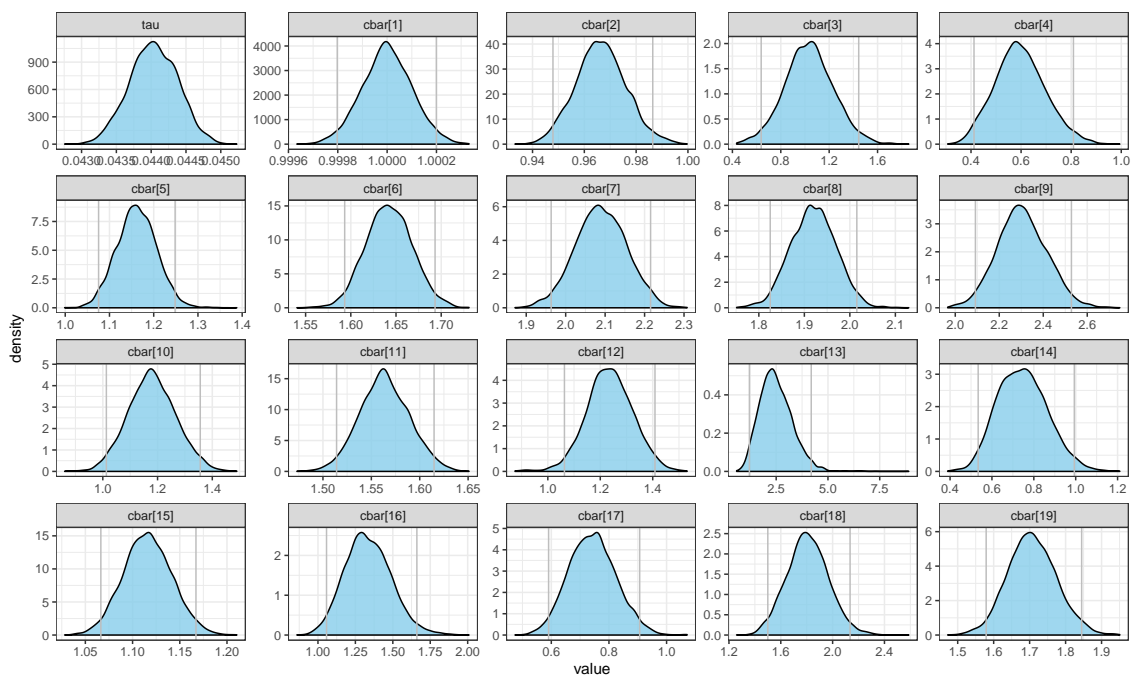


Figure 31:  $\bar{c}s$  for the spatial Random-Effects with Dirichlet estimated infectivity profile.

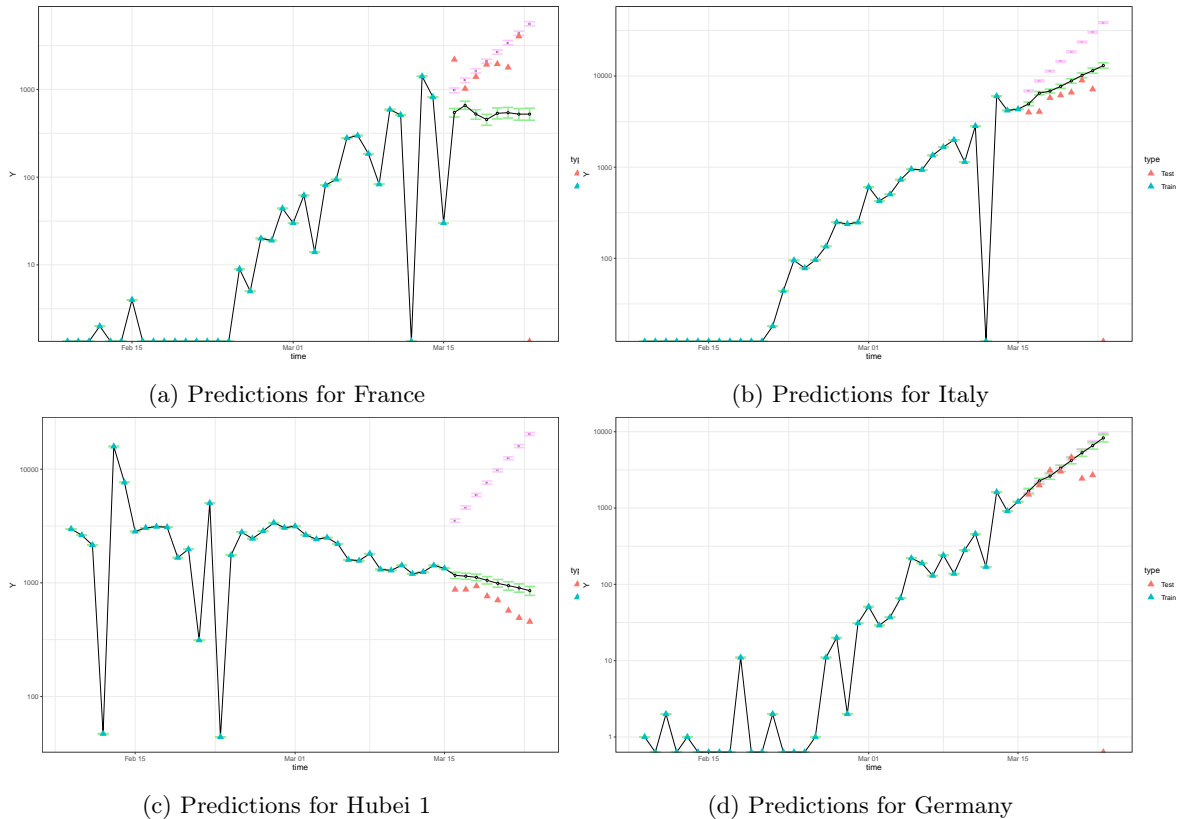


Figure 32: Projection accuracy for a few of the European groups for the spatial Random-Effects with Dirichlet estimated infectivity profile.

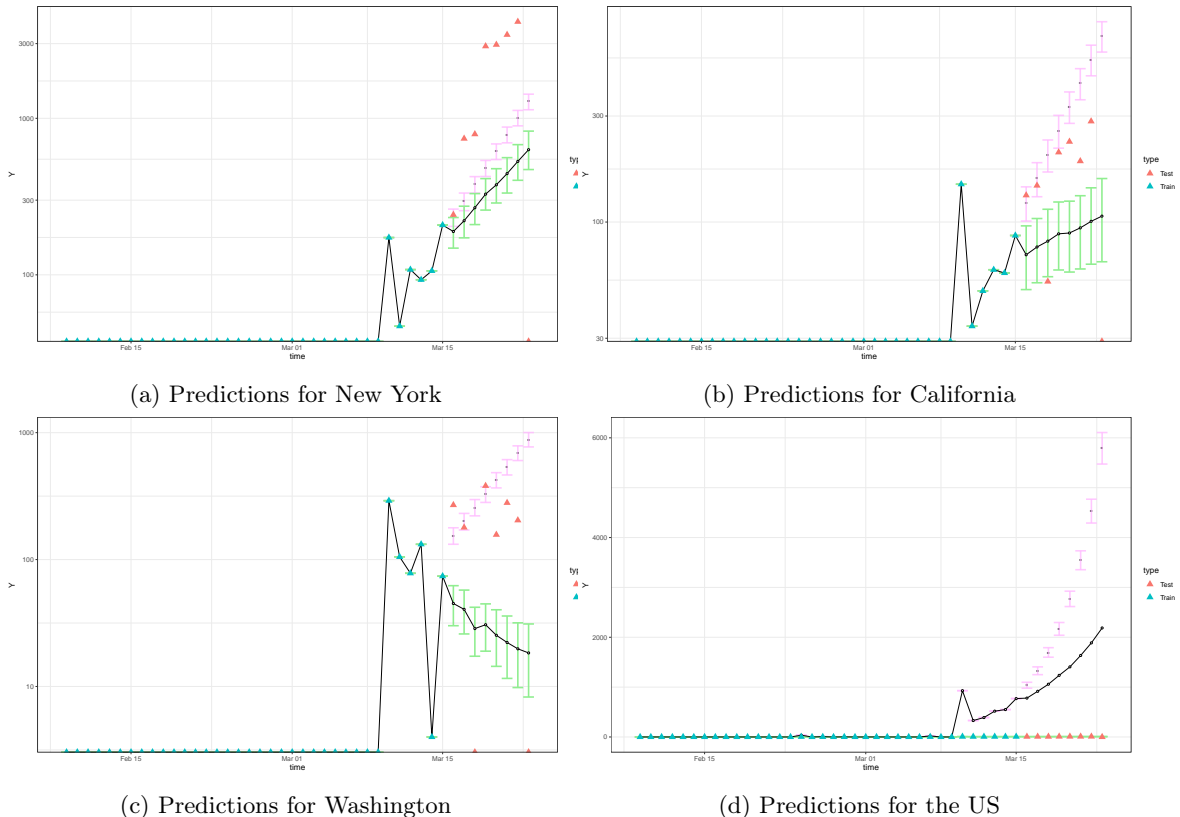


Figure 33: Projection accuracy for groups in the United States for the spatial Random-Effects with Dirichlet estimated infectivity profile.